International Journal of Sediment Research 39 (2024) 355–374

Contents lists available at ScienceDirect

International Journal of Sediment Research

journal homepage: www.elsevier.com/locate/ijsrc

Original Research

Sand sheets—the major dust source in the western Lake Urmia playa—A comprehensive study of the soil-dust properties and stabilization

Nikou Hamzehpour [a,*], Gholam Reza Mahdavinia [b], Mehdi Rahmati [a,c]

[a] Department of Soil Science and Engineering, Faculty of Agriculture, University of Maragheh, Maragheh, 55181-83111, Iran
[b] Department of Chemistry, Faculty of Science, University of Maragheh, Maragheh, 55181-83111, Iran
[c] Institute of Bio and Geosciences (IBG), Forschungszentrum Jülich, Jülich, 52428, Germany

ARTICLE INFO

Article history:
Received 7 July 2023
Received in revised form
20 February 2024
Accepted 6 April 2024
Available online 16 April 2024

Keywords:
Aerosols
Aragonite
Crust stability
Optimum moisture content
X-ray fluorescence (XRF)

ABSTRACT

Climate change accelerated by anthropogenic activities has led to the shrinkage and eventually disappearance of salt lakes all over the world. Gradual desiccation of Lake Urmia (LU) in northwestern Iran, as one example of desiccating lakes, has led to the exposure of the lakebed sediment with enormous dust emission potential in some parts. Sand sheets of western LU are identified as one of the major contributors to aerosols in this region. Yet, dust blown from this area is not well characterized. The aims of the current study were, therefore, to comprehensively investigate the origin of dust from sand sheets; the characteristics of dust and temporal variability of the aerosol and to test the effectiveness of the application of sodium alginate (SA) on soil crusting and stabilization. Soil samples were collected from the two prevailing soil types from sand sheets in August 2020. Dust samples were also collected during four time periods: July and August (the beginning of the dry season); October and November (the beginning of the wet season). Using SA with varying concentrations and different methods of application, the effectiveness of the induced crusts was investigated. Authigenic aragonite minerals with elongated needle shapes were found to be the major constituent of the soil and dust samples. Temporal variability of the dust characteristics and their elemental correlation to dust sources revealed that while dust source 1 (DS_1) with higher clay, salt, and silt contents contribute more to the dust composition from July to August ($R^2 > 0.75$ for DS_1 versus $R^2 > 0.58$ for DS_2), dust source 2 (DS_2) with less salinity and higher sand content becomes the major contributor to dust composition from October to November ($R^2 > 0.91$ for DS_2 versus $R^2 > 0.75$ for DS_1). Results of stabilizing both DS_1 and DS_2 showed that SA-induced crusts on DS_1 are more stable than DS_2 due to the presence of higher clay, silt, salt, organic matter, and lower aragonite minerals. SA-induced crusts by a compaction method significantly performed better than a spray of SA on either dry (DSp) or soil at its optimum water content (WSp) at all concentrations. Nevertheless, spray methods are more feasible at the field scale and in both DSp and WSp methods, $SA_{0.5}$ improved the crust thickness. Scanning electron microscope-energy dispersive X-ray spectroscopy (SEM-EDX) along with thermogravimetric analysis (TGA) confirmed the remaining SA on the soil surface three months after its application indicating the effective performance of the SA solution in sand sheets stabilization. Hence, its application at the field scale could possibly reduce aerosol release and transport to surrounding areas.
© 2024 International Research and Training Centre on Erosion and Sedimentation. Publishing services by Elsevier B.V. on behalf of KeAi Communications Co. Ltd. This is an open access article under the CC BY-NC-ND license (http://creativecommons.org/licenses/by-nc-nd/4.0/).

1. Introduction

Climate change accelerated by adverse effects of human activities on natural resources has led to land degradation including the shrinkage of salt lakes in arid and semi-arid regions worldwide such as Great Salt Lake and Owens Lake in the U.S.A, Aral Sea in Kazakhstan, and Tus Golu Lake in Turkey (Aladin et al., 2009; Bacon et al., 2006; Fraccaro, 2009; Kilic & Kilic, 2010; Wurtsbaugh & Sima, 2022). Lake Urmia (LU) in northwestern Iran is one of the several dried salt lakes in Iran, adversely influenced by both climate variation and anthropogenic activities (Eimanifar & Mohebbi, 2007; Lak et al., 2021; Rashki, Kaskaoutis, et al., 2013; Rezaian Langerodi et al., 2016).

* Corresponding author.
E-mail address: nhamzehpour@maragheh.ac.ir (N. Hamzehpour).

https://doi.org/10.1016/j.ijsrc.2024.04.003
1001-6279/© 2024 International Research and Training Centre on Erosion and Sedimentation. Publishing services by Elsevier B.V. on behalf of KeAi Communications Co. Ltd. This is an open access article under the CC BY-NC-ND license (http://creativecommons.org/licenses/by-nc-nd/4.0/).

LU is the largest salt lake in Iran and the world's second-largest hypersaline lake (Shadkam et al., 2016). Since the start of its desiccation two decades ago, dust frequency has increased in northwestern Iran (Ahmady-Birghani et al., 2020; Boroughani et al., 2019; Sotoudeheian et al., 2016). By 2022, approximately 90% of the lake has vanished within a few decades promoting the formation of the LU playa (LUP) in the vastly exposed lake bed sediment. The major identified and studied playa surfaces of LUP are clay flats, clay flats-salt crusts, sandy salt crusts, puffy grounds, and sand sheets (Hamzehpour et al., 2022; Kheirfam, 2022; Motaghi et al., 2020; Taghizadeh-Mehjerdi et al., 2021). Among these playa surfaces, sandy salt crusts are the major dust sources in the southeast (Kheirfam, 2022; Motaghi et al., 2020), puffy grounds in the south (Alkhayer et al., 2019), and sand sheets in the west of LUP (Ahmady-Birghani et al., 2018; Hamzehpour et al., 2022; Kheirfam, 2022).

In the absence of soil-protecting factors, mineral soil particles can be displaced by wind and transported over long distances. Besides their adverse effects on human health and environmental safety (Hassan et al., 2021; Molina et al., 2020; Rai, 2015, 2016), they can significantly impact the climate globally by affecting the earth's radiation budget (Bishop et al., 2002; Clarke et al., 2001; Froyd et al., 2022; Middleton, 2017; Schepanski, 2018). There are several soil and environmental factors which can affect dust emission from a specific land surface. While vegetation cover (Galloza et al., 2018; Li et al., 2007; Pierre et al., 2012; Tegen et al., 2002) and soil moisture (Ju et al., 2018; Kim & Choi, 2015; Munkhtsetseg et al., 2016) are the environmental factors that can control the detachment of soil particles by wind, intrinsic soil properties such as clay, silt, and organic matter can prevent windblown aerosols by increasing adhesiveness of the soil particles and creating larger aggregates (Colazo & Buschiazzo, 2010; Warrence et al., 2002; Zobeck et al., 2013). The development of a surface crust by any kind of process (physical, chemical, and biological) can also have a protective role against wind erosion (Nield et al., 2015; Ries et al., 2014; Yan et al., 2015).

Various physical, chemical, and biological methods have been developed to stabilize erodible lands and control dust. Physical methods include the construction of wind breakers, the application of clay and mulch, chemical methods involving usage of cementing materials and chemical compounds such as sodium, calcium, magnesium chlorides, and calcium sulfate; and biological methods including use of organic materials or organisms (Afrin, 2017; Belnap & Büdel, 2016; Firoozi et al., 2017; Ingles & Metcalf, 1972; Saldanha et al., 2018).

To improve the stability against wind or water erosion, some polymers such as urea-formaldehyde with sulfuric acid (H_2SO_4) as a cross-linker agent (Yang et al., 2007), polymerized vinyl acetate (Liu et al., 2012), alkyl acrylates (Lahalih & Ahmed, 1998), polyvinyl acetate, acrylic polymer, and styrene–butadiene latex (Siddiqi & Moore, 1981) have been introduced. The application of these polymers proved their cementing ability to aggregate sand particles and form chemical crusts on desertified land. However, most of the polymer hydrogels are made from monomers or polymers of acrylic acid and polyacrylamide which are derived from petroleum production, and, thus, they persist for a long period of time in the environment (e.g., Wilske et al., 2014) and also are toxic for humans or animals (Takigami et al., 1998).

Polysaccharides and their derivatives, due to their unique properties such as biodegradability, environmental and ecological friendliness, low cost, and easy availability are good replacements for hydrogels produced from petroleum products (Beaucamp et al., 2019; Guilherme et al., 2015). Sodium alginate (SA) is a natural polysaccharide which is widely used in food and medical industries. It has favorable film-forming properties and often is applied in coating and biopolymer film (Chan et al., 2006). Furthers, SA films are hydrophilic matrices through which water molecules can easily pass. During the past few years, there have been studies on the effect of SA application on soil surfaces to improve surface resilience against wind and water erosion through the formation of stable crusts. SA films also could be used as a substitute for traditional soil stabilizers, as they are more environmentally friendly than cement or lime (Almajed et al., 2020; Lemboye et al., 2021). Zhao et al. (2020) showed that the use of SA on loess soil resulted in the formation of larger aggregates by flocculating soil particles by filling the pores between them. SA could also improve the strength, shear parameters, and water stability of loess. Wade et al. (2021) found that using SA on a soil surface improved soil aggregate diameter 1.5 times through which soil susceptibility to wind erosion decreased. Similar results also have been reported by other researchers (Arab et al., 2019; Lemboye et al., 2021; Peng et al., 2017).

Sand sheets of the western LU are the most important dust source in the region located about 1 km from Jabal Kandi village, where 2000 ha of the land has turned into moving sand. This area has become a serious threat to nearby agricultural fields, orchards, and villages. Jabal Kandi also is known as one of the active centers of dust generation which can then extend in the direction of the prevailing winds to cities such as Urmia and its suburbs with an approximate population of one million people. Since the desiccation of LU and activation of several dust hotspots, there have been attempts to stabilize dust sources by the establishment of native vegetation cover. However, initial plant establishment needs periodic and regular irrigation which is expensive and time-consuming. Yet, some of these projects were not successful in the region, leading to wilting and death of plants at the early stages of growth.

Based on previous studies (Hamzehpour et al., 2022; Hamzehpour & Marcolli, 2024; Taghizadeh-Mehrjerdi et al., 2021), two soils with different characteristics have been identified within sand sheets of the western part of LU, which are named dust source 1 (DS_1) and dust source 2 (DS_2) throughout the current paper. Both DS_1 and DS_2 soils have a high content of wind erodible material and are considered as dust sources. However, they have different physicochemical characteristics along with the presence of a fragile soil curst on the surface of DS_1 which is absent in DS_2 (Fig. 1(e)). Overall, the contribution of each soil to the dust composition is not clearly known. Therefore, the current study aims at i) a detailed investigation of the major soil types of the sand sheets; their contribution to dust composition in the region as well as correlation to particulate matter 10 μm or less in diameter (PM_{10}) in the Urmia city; ii) evaluation of the efficiency of SA application in the stabilization of sand sheets.

2. Materials and methods

2.1. Study area

The study area is located between 45° 06′ to 45° 23′ E and 37° 19′ to 37° 56' N, 35 km north of Urmia city, in the vicinity of Jabal Kandi village and on the western edge of LU (Figs. 1(a) and 1(b)). The area is approximately 2000 ha and has been classified as a sand sheet playa surface in previous studies (Hamzehpour et al., 2022; Taghizadeh et al., 2021). Sand sheets of the region are composed of more than 80% wind-erodible fractions and are responsible for regional dust since catastrophic desiccation of LU (Figs. 2(a)–2(d)).

2.2. Meteorological data

Daily wind speed (WS) and wind direction (WD) along with 24-h rainfall data for the dust collection dates, as well as average

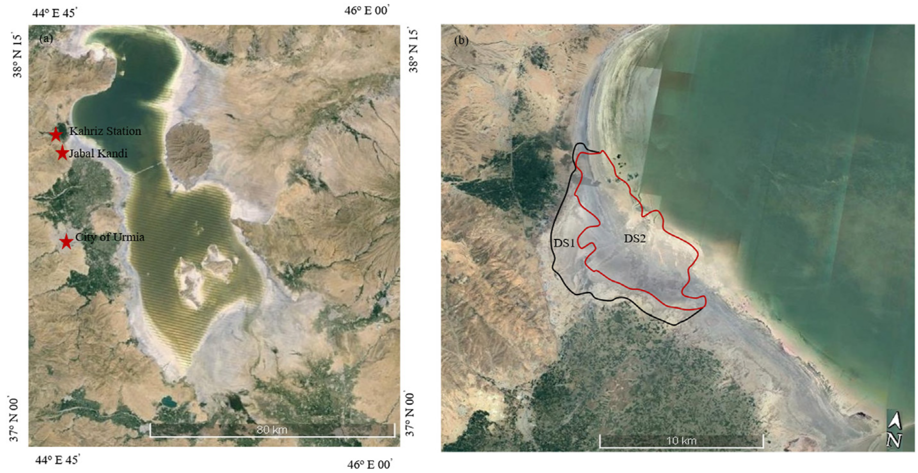

Fig. 1. (a) LU in northwestern Iran and location of study area and Kahriz weather station near Jabal Kandi village in the western part of LU. (b) Location of two investigated soil types in vicinity of Kahriz station. The area shown in black polygon represents DS_1 while area in red represents DS_2.

values for the sampling months (July to November 2020) for the Kahriz station (5 km away from the study area), were obtained from the National Climatic Center website (https://data.irimo.ir/). Particulate matter smaller than 10 μm (PM_{10}) measured hourly for Urmia city also was obtained from the Department of the Environment of West Azerbaijan province. A summary of the mythological data is listed in Table 1.

To investigate the correlation between WS and WD with PM_{10} in Urmia City (35 km southwest of the study area), three-hourly WS and WD data were obtained from the National Climatic Center website (https://data.irimo.ir/) for the Urmia station from July to November 2020 which were used along with PM_{10} data in a correlation wavelet analysis (see Section 2.6).

2.3. Soil and dust sampling

In August 2020 (the hottest month of the year in this region) (Fig. 3), composite soil samples were taken from both dust sources at a depth of 0–5 cm. To prepare composite soil samples, from each source separately, 10 soil samples were collected from different parts and then were mixed to obtain a unified sample for subsequent analysis.

Fig. 2. (a) Sand sheets of western part of LU and established vegetation cover to control sand movement and dust detachment. (b) Dust blowing from sand sheets during a normal day. (c) White arrow marks depth of windblown soil surface. (d) Thin surface crust at surface of DS_1.

Table 1
PM_{10} concentration, WS, WD, and 24 h rainfall data for sampling dates at Kahriz station as well as average values for study months in 2020. PM_{10} values are recorded at Urmia, 35 km southwest of sand sheets.

	Unit	Sampling date				Monthly average			
		9th Jul.	18th Aug.	8th Oct.	1st Nov.	Jul.	Aug.	Oct.	Nov.
PM_{10}	μg/m^3	53.6	87.2	102.9	22.1	70.1 ± 15	62.1 ± 21	38.2 ± 18	36.8 ± 15
WS	m/s	9	9	10	11	5.7 ± 2	6.0 ± 4	6.5 ± 3	5.7 ± 2
WD	(°)	290	270	270	260	247 ± 73	193 ± 110	206.1 ± 90	194 ± 100
24 h rainfall	mm	0	0	0	0	0.02 ± 0.1	0.11 ± 0.5	0.83 ± 1.5	6.23 ± 2.2

Note: ± is plus or minus of standard deviation value.

Dust samples were collected in four different time periods: 2 months at the beginning of the dry season, namely dust July (D_J) and dust August (D_A), and 2 months at the beginning of the wet season namely dust October (D_O) and dust November (D_N) in 2020 (Fig. 3). At each dust sampling time, aerosol particles in the vicinity of sand sheets were collected using BSNE sediment traps 2 m above the ground.

2.4. Soil–dust analysis

2.4.1. Physicochemical analysis

Collected soil and dust samples were moved to the soil laboratory at the University of Maragheh, East Azerbaijan, Iran. Then the soil samples were air-dried and subjected to several physical and chemical analyses. Prior to these analyses, soil samples were passed through a 2 mm sieve, while dust samples were kept unaltered as wind normally detaches, suspends, and carries soil particles smaller than 2 mm, mostly in the size of fine sand (200–50 μm), silt (2–50 μm), and clay (< 2 μm) (collected by dust samplers).

Soil electrical conductivity (EC) and acidity (pH) were measured in a 1 : 2.5 soil-to-water extracts using a Jenwey conductivity meter (model 4510) and VWR Symphony SB70P pH meter, respectively (Rhoades, 1996). Soil organic carbon (OC) was determined using the wet oxidation technique (Nelson & Sommers, 1996); and soil total carbonates (TC) were quantified using a back titration of remaining hydrochloric acid (HCl) (Page et al., 1982).

The particle size distribution (PSD) was measured with a laser diffraction size analyzer (LDSA; model LS 13320) for particle sizes between 0.4 and 2000 μm for the collected soil and dust samples. To disperse the samples, they were wet sonicated for 5 min prior to analysis (Dane & Topp, 2020). The classification of soil fractions in size classes was done based on the criteria defined by the American Society for Testing and Materials (ASTM, D-2487, 2000).

2.4.2. X-ray fluorescence (XRF)

To determine XRF analysis, soil and dust samples were decreased to diameters lower than 53 μm by milling and analyzed in an energy-dispersive XRF spectrometer Shimadzu, with a Rh source (Prandel et al., 2014). The collection time was 100 s with energy bands between 8 and 40 kV. The XRF analysis was done by Mahamax Laboratory in Tehran (https://mahamax.com/).

2.4.3. Thin section preparation for polarized microscopy

Two soil samples from investigated dust sources were used for micromorphological studies. Vestpal resin with cobalt as a catalyst and stearic acid as a hardener was used to impregnate the soil samples. The thin sections were polished to a thickness of approximately 20–30 μm. An Olympus BH2 petrographic microscope was used for thin section observations.

2.5. Crust development using sodium alginate

Soil samples from the two dust origins (DS_1 and DS_2) were air-dried and then passed through a 2 mm sieve to exclude any larger substances. Then two different methods of sodium alginate (SA) application were used. The first method was spraying of SA solution (Sp) on the soil surface. The second method was mixing the SA solution with soil and then compaction (MC).

In Fig. 4, the Fourier transform infrared (FTIR) spectrum of commercial SA powder used for soil stabilization in the range of 400–4,000 cm^{-1} along with the representative peaks for the sodium alginate bonds are given.

To investigate the primary soil moisture effect on increasing SA solution efficiency, the SA surface spray was applied once on top of dry soil (DSp) and once again on the soil surface with the moisture content at field capacity (WSp). The SA solution was prepared by dissolving SA powder first in distilled water at room temperature and then heating the solution to 85 °C mixing with a magnet stirrer to produce a uniform SA solution with target concentrations of 0.5%, 1%, and 2%. The dry soil-to-solution ratio in all treated soils was the optimum moisture content.

2.5.1. Penetration test

To examine the surface strength of biopolymer-modified soil samples with varying SA concentrations, an automatic micro penetrometer (model MP11, Iran) with a needle penetrometer was used to measure the penetration rate and pressure (Fig. 5(a)). Samples were examined with a rate of 0.2 mm to a depth of 5 cm and automatically collected data were used to draw penetration graphs (Fig. 5(b)). The applied maximum pressure was 12,000 kPa.

2.5.2. Thermogravimetric analysis (TGA) and scanning electron microscope (SEM) imaging

Crust samples induced by DSp-SA_1 along with untreated soil samples (DSp-SA_0) were subjected to SEM imaging after 3 months of SA application. To investigate the morphology of the dust samples, two dust samples from July (D_J) and November (D_N) also were subjected to SEM imaging. A 1 × 1 cm crust was placed on a stopper inside a vacuum for 10 min before being coated with a

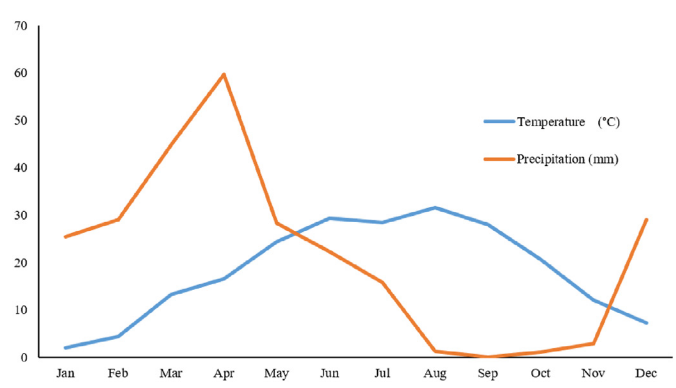

Fig. 3. Monthly changes in temperature and total precipitation during 2020 in Kahriz station near sand sheets of western LU.

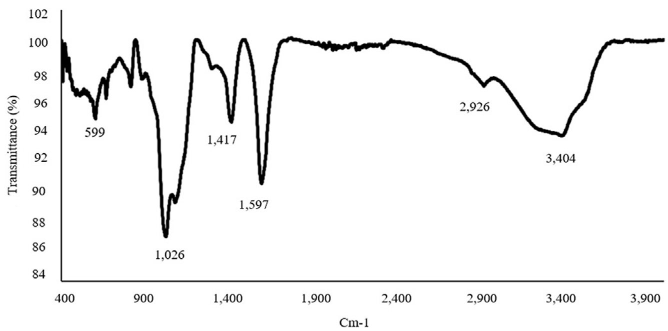

Fig. 4. FTIR spectra of applied SA in the range of 400–4000 cm^{-1} used in sand sheet stabilization.

thin layer of gold to prevent the specimen from charging under the electron beam during imaging. The structure of the crust was characterized using a field-emission scanning electron microscope (FEI QUANTA 200) equipped with energy-dispersive X-ray spectroscopy (SEM-EDX). Soils subjected to SEM analysis also were chosen for thermogravimetric analysis (TGA) coupled with differential scanning calorimetry (DSC) to identify their thermal behavior. TGA analysis was done using STD Q600 from TA instruments. The gas flow was set to 20 mL/min oxygen (O_2) to obtain an atmospheric mixture. A soil sample (10–20 mg) was placed in an aluminum oxide (Al_2O_3) crucible and heated up at a heating rate of 20 °C/min from 40 to 1000 °C. In TGA thermograms, the region of 120–190 °C is a transition between endothermic water loss and exothermic organic matter oxidation. The TGA and SEM analysis were done by the Mahamax Laboratory in Tehran (https://mahamax.com/).

2.6. Statistical design

A full factorial design with three factors (dry spray, wet spray, and compaction); each factor with 4 levels (zero, 0.5%, 1%, and 2%) and three replications was used to investigate the role of SA application on crust resilience to wind erosion characteristics. The experimental data were analyzed using the SAS software 9.1 (SAS Institute Inc, 2006) and the mean comparison was done using Duncan's multiple range test (DMRT) ($p < 0.05$) (Tallarida et al., 1987).

To test the hypothesis that the dust generated in the study area (Jabal Kandi) leads to increased PM_{10} concentration at Urmia (the largest city nearby), a wavelet coherence analysis (WCA) was done between the wind speeds in the north and northeast directions (blown over Jabal Kandi toward the city of Urmia) and the PM_{10} concentration in the Urmia station. For this purpose, the MATLAB (MathWorks Inc., Natick, Massachusetts) software package was used for WCA as introduced by Grinsted et al. (2004) to check the evolution of coherence between two studied variables in both time and frequency domains. The applied package implements wavelet cross-correlation to efficiently determine the degree of correlation and delay between two studied signals on a given scale (Labat, 2005). For details on the use and interpretation of the WCA results, please refer to Rahmati et al. (2020) and Rahi et al. (2023).

3. Results and discussion

3.1. Sand sheets contribution to dust composition and PM_{10}

3.1.1. Soil–dust physicochemical properties

In Table 2, a summary of the physicochemical analysis of the two prevailing soil types (DS_1 and DS_2) from sand sheets from the

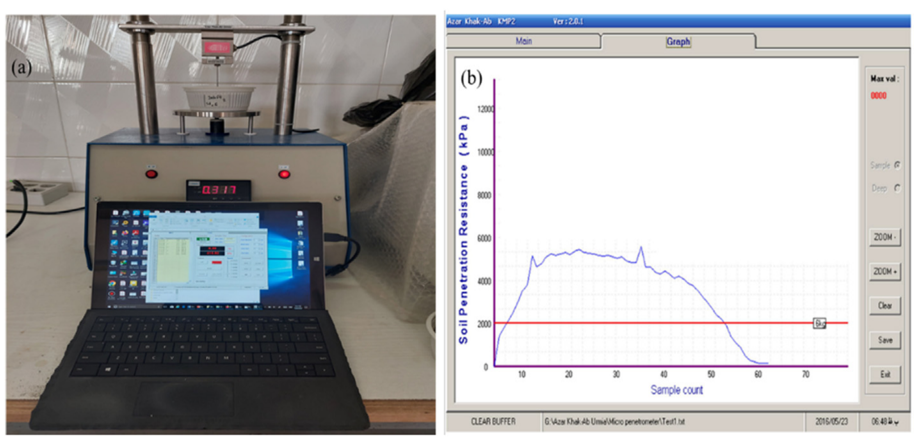

Fig. 5. (a) Automated micro-penetrometer to determine crust compressive strength; (b) soil penetration force (resistance) versus penetration depth graphs.

Table 2
Physicochemical properties of soil and dust samples from sand sheets of the western Lake Urmia.

Sample	EC (dS/m)	TC (%)	OM (%)	pH	Particle size class (< 2 mm)						
					Clay (%)	Silt (%)			Sand (%)		
						Fine	Medium	Coarse	Fine	Medium	Coarse
Dust source 1	23.4	32.2	1.0	8.3	6.5	10.5	5.3	3.5	60.0	14.2	0
Dust source 2	0.39	49.2	0	8.6	1.1	0.5	0.9	0.9	48.1	36.1	12.4
Dust-July	26.0	25.2	1.7	8.6	2.7	1.1	1.7	0.9	56.5	35.1	2.0
Dust-August	43.9	43.0	1.3	8.4	2.9	1.2	0.4	0.4	51.0	43.6	3.4
Dust-October	2.4	38.6	1.2	8.6	0.0	0.7	1.1	0.6	73.4	21.3	2.9
Dust-November	2.8	52.7	1.3	8.5	1.0	0	0	0	66.7	31	1.3

Note: EC refers to the electrical conductivity; TC refers to the total carbonates; OM refers to the organic matter; clay < 2 µm; silt 2–50 µm, with fine (2–5 µm), medium (5–20 µm), and coarse (20–50 µm) fractions; sand 50–2,000 µm, with fine (50–200 µm), medium (200–500 µm), and coarse (500–2,000 µm) fractions.

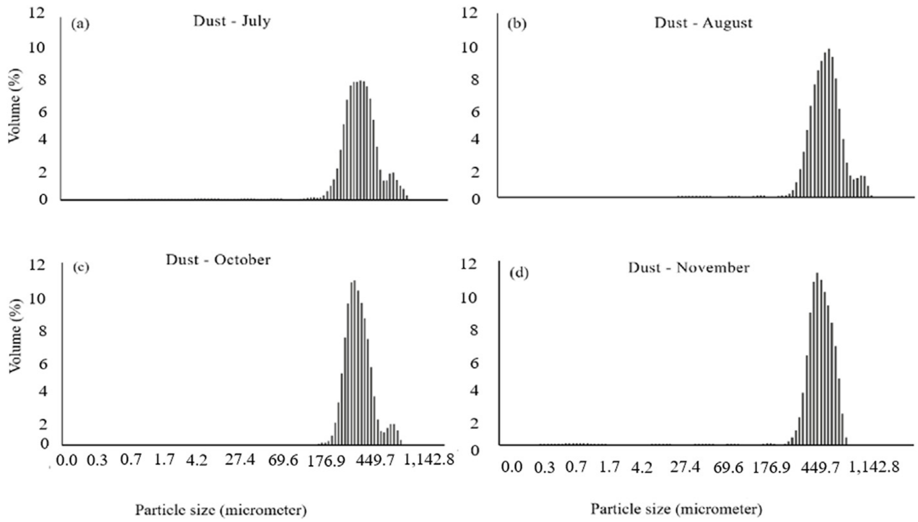

Fig. 6. Particle size distribution analysis of dust samples. Dust sample from (a) July, (b) August, (c) October, and (d) November 2020.

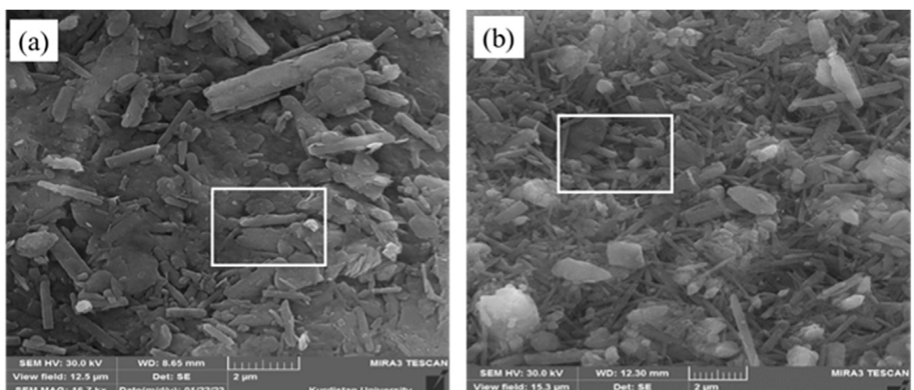

(a)

Elt	Line	Int	Error	K	Kr	W%	A%
C	Ka	9.2	3.5106	0.0469	0.0343	8.32	17.52
O	Ka	54.3	3.6266	0.0852	0.0624	22.53	35.61
Na	Ka	50.9	0.6600	0.0291	0.0213	3.26	3.59
Mg	Ka	7.3	0.6701	0.0040	0.0029	0.38	0.39
Si	Ka	54.0	0.5722	0.0327	0.0239	2.62	2.36
Cl	Ka	131.2	2.4016	0.1293	0.0947	10.07	7.19
Ca	Ka	422.1	0.8289	0.6728	0.4926	52.81	33.33

(b)

Elt	Line	Int	Error	K	Kr	W%	A%
C	Ka	12.7	4.7199	0.0289	0.0225	3.64	8.44
O	Ka	103.9	4.8759	0.0728	0.0569	22.40	38.98
Na	Ka	4.2	2.3092	0.0011	0.0008	0.13	0.16
Mg	Ka	27.1	2.3445	0.0066	0.0052	0.67	0.77
Si	Ka	110.2	0.6964	0.0298	0.0232	2.54	2.52
Cl	Ka	25.1	0.5332	0.0110	0.0086	0.89	0.70
Ca	Ka	1194.4	1.1111	0.8498	0.6635	69.72	48.43

(c)

Elt	Line	Int	Error	K	Kr	W%	A%
C	Ka	14.9	8.9678	0.0404	0.0273	4.40	8.76
O	Ka	198.4	9.2643	0.1655	0.1121	37.57	56.14
Na	Ka	2.0	0.7944	0.0006	0.0004	0.07	0.07
Mg	Ka	5.2	0.8065	0.0015	0.0010	0.14	0.13
Si	Ka	42.5	3.2195	0.0137	0.0093	1.03	0.88
Cl	Ka	42.2	438.645	0.0221	0.0150	1.60	1.08
Ca	Ka	893.3	0.8487	0.7562	0.5123	55.20	32.93

(d)

Elt	Line	Int	Error	K	Kr	W%	A%
C	Ka	30.5	5.3200	0.0638	0.0450	7.26	14.65
O	Ka	192.0	5.4959	0.1234	0.0871	30.87	46.80
Na	Ka	7.2	0.7558	0.0017	0.0012	0.19	0.20
Mg	Ka	35.8	0.7674	0.0081	0.0057	0.75	0.74
Si	Ka	137.4	2.0233	0.0340	0.0240	2.67	2.31
Cl	Ka	17.3	0.5954	0.0070	0.0049	0.52	0.36
Ca	Ka	1168.0	1.0280	0.7620	0.5376	57.74	34.94

Fig. 7. SEM images along with EDX analysis of soil and dust samples from sand sheets: (a) DS_1, (b) DS_2, (c) D_J, and (d) D_N. Note: C is carbon, O is oxygen, Na is sodium, Mg is magnesium, Si is silica, Cl is chloride, and Ca is calcium; Elt refers to the element; K refers to the spectral line name; Kr is *k*-ratio, the ratio of unknown intensity relative to a reference intensity; W% is weight percent, as a function of weight; A% is atomic percent, as a function of the number of atoms.

western LU along with the collected dust samples near this region during July–November 2020 are listed. In Fig. 6, the particle size distribution of the dust samples is shown. Based on the results listed in Table 2, DS_1 and DS_2 were different by means of their electrical conductivity (EC), total carbonates content (TC), organic matter (OM), and PSD. DS_1 had relatively higher EC (23.4 versus 0.39 dS/m) and OM (1.0% versus 0%) in comparison to DS_2 while the TC content of DS_2 was higher than that of DS_1 with 49.2% versus 32.2%.

Dust samples collected near these two dust sources also showed distinct variations through time. While EC values from August (D_A) and July (D_J) at the beginning of the dry season were high (26.0 and 43.9 dS/m, respectively), dust samples from October (D_O) and November (D_N) had relatively low EC values (2.4 dS/m and 2.8 dS/m) representing their low salt content. TC content of the dust samples increased from 25.2% in D_J to 52.7% in D_N. The OM content of all dust samples was almost identical with a mean value of 1.4% that was higher than the OM content of their corresponding sources. Considering PSD of the dust samples, they consisted of high sand and low silt and clay fractions. Generally, the insignificant contribution of the clay and silt fractions to dust composition, is mostly related to their aggregation to larger particles on the ground with more resilience against wind force, preventing them from detachment, and resulting in their lower content in dust in comparison to their origins.

D_J and D_A were composed of a wider range of particle size classes than D_O and D_N. Fine and medium sand fractions were the predominant particle sizes in all dust samples, with the medium sand size being higher in the dust samples from July and August, while fine sand dominated in the dust samples from October and November (Fig. 6).

3.1.2. Dust source morphology

In Fig. 7, SEM images of the soil samples from both dust sources (Fig. 7(a): DS_1 and Fig. 7(b): DS_2) and dust samples (Fig. 7(c): D_J and Fig. 7(d): D_N) along with their EDX analysis are shown. The distinguishable elongated, needle shape minerals dominating the samples, are identified as aragonite minerals (Bermanec et al., 2009). In fact, aragonite is one of the main authigenic minerals in the LU sediment formed due to the high magnesium/calcium (Mg/Ca) molar ratio in LU brine as well as changes in temperature, evaporation, and shifts in carbon dioxide (CO_2) balances induced by biological activity (Kelts & Hsü, 1978; Kelts & Shahrabi, 1986). The most dominant forms of aragonite in LU sediment are reported to be micrite aragonite, fecal pellets (composed of more than 80% aragonite), and ooid-like coated grains. Detailed studies of the authigenic aragonite forms in the sediment of LU are given by Kelts and Shahrabi (1986) and Sharifi et al. (2018).

Taking into consideration Fig. 7, aragonites in DS_2 are slenderer, more well-formed needles with smaller sizes and tapered ends (Fig. 7(a)) than those observed in DS_1 where aragonites are more irregular in shape with frayed ends (Fig. 7(b)). These differences in the morphology of the aragonites indicate the variable circumstances under which sediment of these two soil types have formed. Overall, aragonite minerals in the dust samples were more irregular, and smaller in size with less crystallinity than those in the soils.

In Fig. 8, images of the soil samples under a microscope and cross-polarized light (XPL) are shown. Aragonite minerals in both soil samples are in the form of ooids which is the most common non-skeletal component of limestone. They are normally characterized by enveloping laminations and are the product of calcite

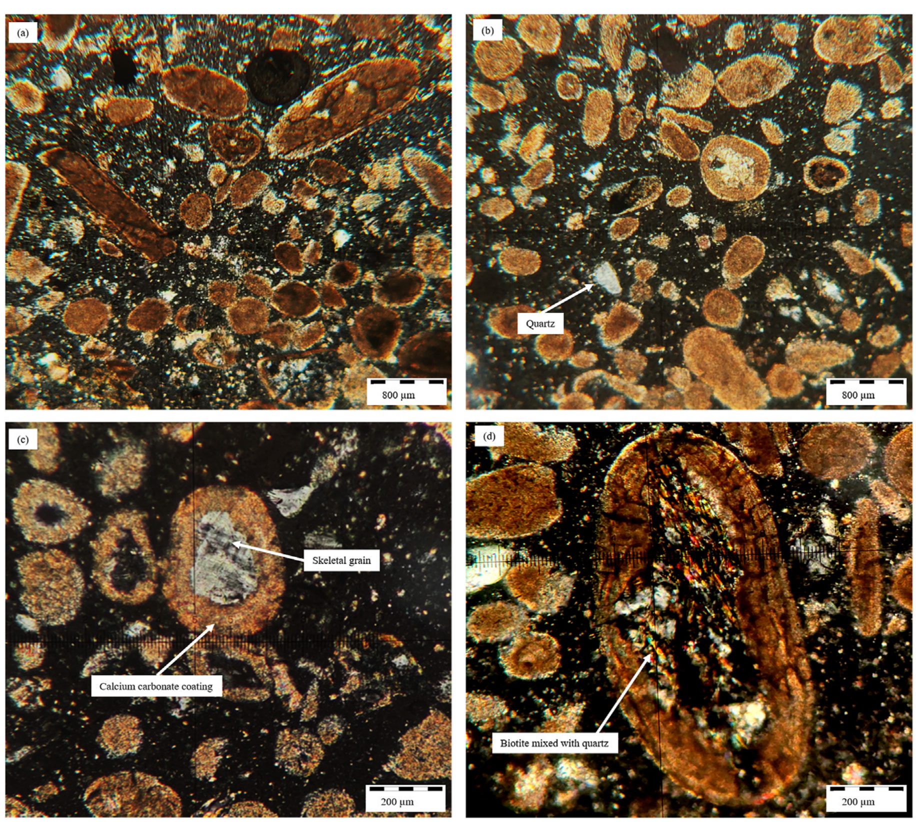

Fig. 8. Images of DS_1 and DS_2 soil samples from sand sheets under microscope and cross-polarized light (XPL). (a) and (c) DS_1 with 4X and 20X magnifications, respectively; (b) and (d) DS_2 with 4X and 20X magnifications, respectively.

and aragonite precipitation under the influence of biological activity at the sediment-water interface. Ooids are spherical to sub-spherical grains, formed of micro-size calcite or aragonite crystals organized tangential to grain surfaces. In Figs. 8(c) and 8(d), aragonite concentration around the quartz (Fig. 8(c)) and biotite mixed with quartz (Fig. 8(d)) grains are clearly distinguishable.

Sharifi et al. (2018) reported that in most cases, ooid-like coated grains are polished fecal pellets of artemia, covered with a single or multiple layers of aragonite crystals. In line with Sharifi et al. (2018), sand sheets of western LU are composed of multiple concentric layers of aragonite crystal coatings, superimposing a primary skeletal grain such as quartz, feldspar, or biotite minerals.

3.1.3. Sand sheets contribution to dust composition

XRF results for the studied soil and dust samples are shown in Fig. 9. Calcium (Ca) was the predominant element in all the samples with a mean value of 50.2%; a minimum value of 40.1% in D_J and maximum value of 62.2% in DS_2. As discussed in the previous section, the considerably high content of the Ca could be related to the presence of calcium carbonate minerals in the form of aragonite in the samples. Silica (Si) is the second prevailing element in the samples with a mean value of 9.6%. The sodium (Na) content of the samples was variable with greater content in DS_1, D_J, and D_A. The sodium/calcium (Na/Cl) ratio was almost equal to 1, showing that NaCl is the dominant mineral form of Na in the samples. Strontium (Sr) also was detected as one of the prevailing elements among the samples which also is one important tool to distinguish aragonite from calcite where high concentrations of the large cations such as Sr in aragonite minerals are more common than in calcite minerals (Bermanec et al., 2009).

In a previous study, by using quantitative mineralogy, it was reported that 52.8% and 56% of the total non-clay fraction of the soil and dust samples from the sand sheets are composed of quartz, calcite, aragonite, and halite (Hamzehpour et al., 2022). Generally, calcite, quartz, clay minerals, and gypsum are reported to be the main constituents of atmospheric particles in western Iran. The high calcium carbonate ($CaCO_3$) minerals' content of the dust samples is related to the calcareous soils of the region (Ahmady-Birgani et al., 2015). Quartz and carbonate minerals were found to be the prevailing constituents of atmospheric dust in other studies

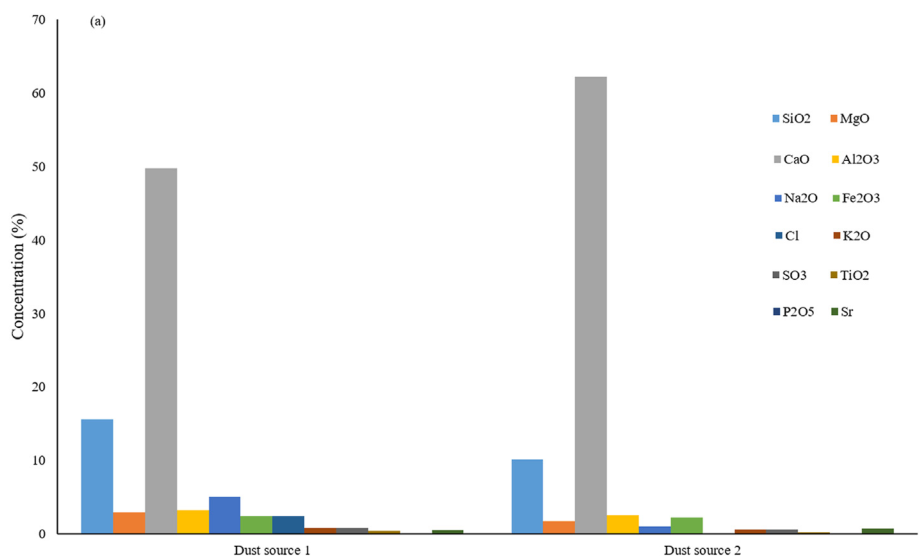

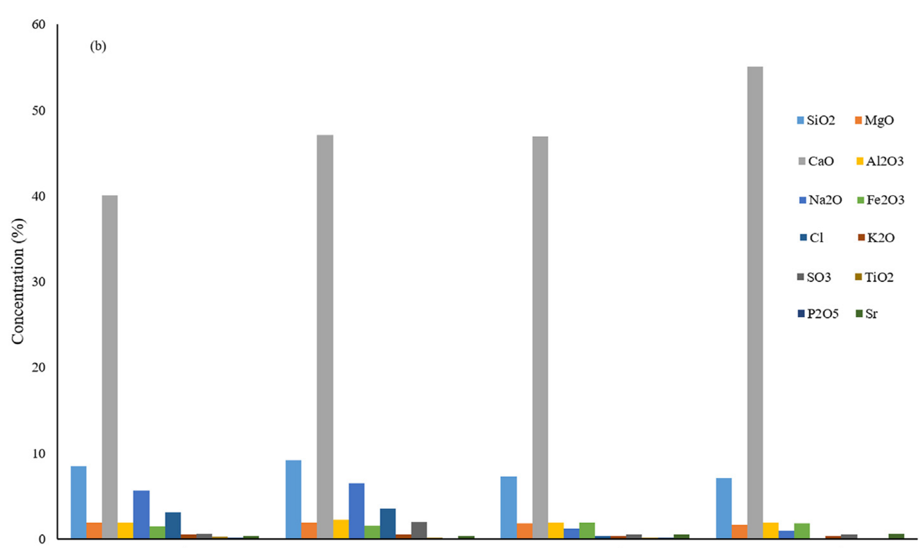

Fig. 9. Results of XRF analysis for prevailing elements in the samples. (a) Soil samples; (b) dust samples. Note: SiO_2 is silicon dioxide, MgO is magnesium oxide, CaO is calcium oxide, Al_2O_3 is aluminum oxide, Na_2O is sodium oxide, Fe_2O_3 is ferric oxide, K_2O is potassium oxide, SO_3 is sulfur trioxide, TiO_2 is titanium oxide, and P_2O_5 is phosphorus pentoxide.

in arid and semi-arid regions throughout the world (Al-Dabbas et al., 2012; Díaz-Hernández et al., 2011; Jiries et al., 2002; Rashki, Eriksson, et al., 2013; Zarasvandi et al., 2011).

To better understand the contribution of the identified dust sources from sand sheets to dust composition, the coefficient of determination (R^2) between elements in the soil and dust samples was calculated and shown in Fig. 10. Overall, the high correlation between the elemental concentrations in the soil and dust samples (R^2 > 0.75) demonstrate that the selected soil samples are indeed main sources of the airborne dust, evidencing the local contribution of the soils to the dust in the region. However, higher R^2 for DS_1 during July (0.95 versus 0.84 in DS_2)

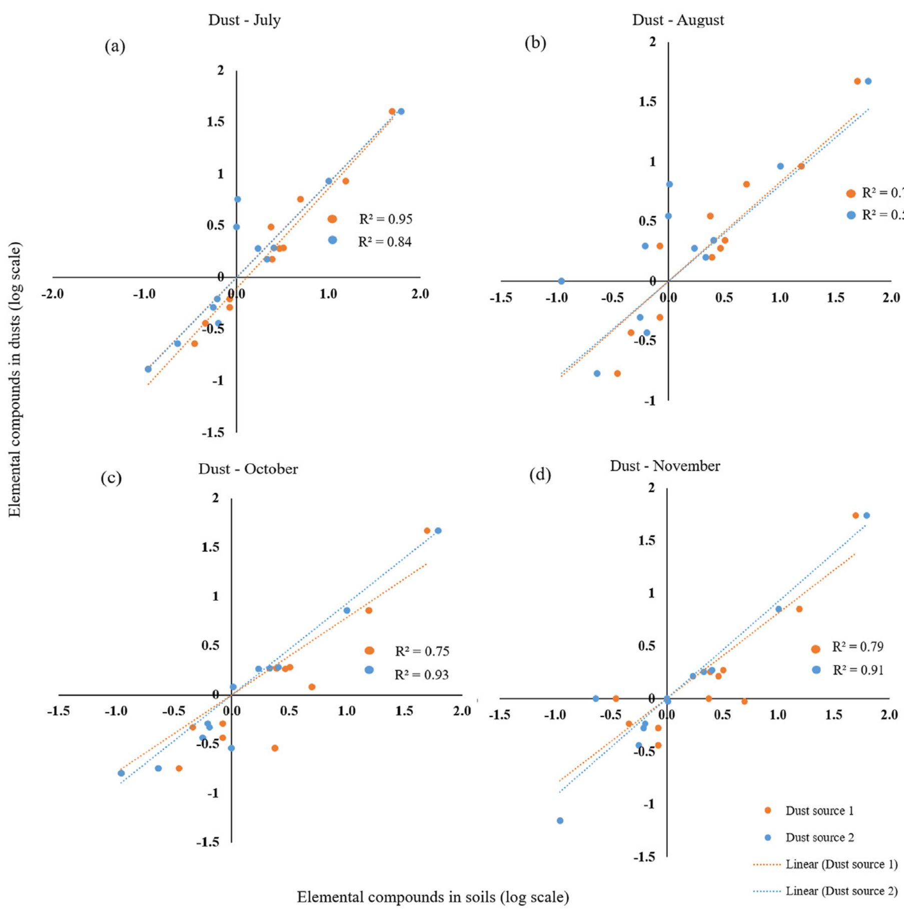

Fig. 10. Correlation between elemental concentrations in soil and dust samples. (a) Dust July (D_J); (b) dust August (D_A); (c) dust October (D_O); (d) dust November (D_N).

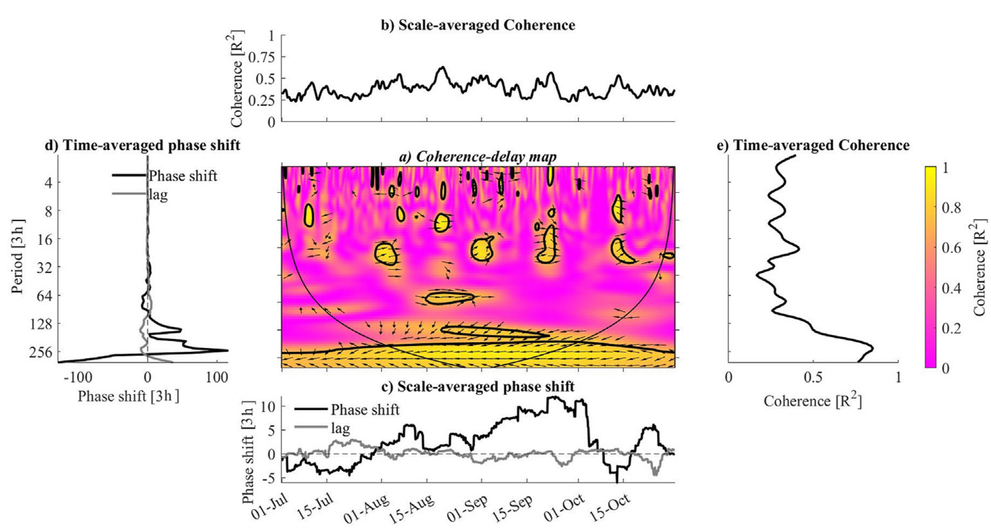

Fig. 11. Coherence-delay plots between PM_{10} at Urmia station and wind speed from the north and northeast which is blown over sand sheets toward the city of Urmia. (a) Coherence-delay map, (b) scale-averaged coherence, (c) scale-averaged phase shift, (d) time-averaged phase shift, and (e) time-averaged coherence.

and August (0.75 versus 0.58 in DS_2) and on the contrary, greater values for DS_2 during October (0.93 versus 0.75 in DS_1) and November (0.91 versus 0.79 in DS_1) confirms that at the beginning of the dry season in the region, DS_1 plays more significant role in dust composition while towards the end of the dry season, DS_1 becomes less active and DS_2 acts as the sole contributor to dust composition.

Based on the field observations, towards the middle and end of the dry season, salt deposition on the surface of DS_1 simultaneously with the extreme water evaporation leads to the formation of a thin layer of salt crust on the soil surface which in combination with the clay, silt, and organic matter, protects DS_1 against further erosion. However, during the wet season, re-dissolution of the salt and its dislocation to the lower layers, re-activates DS_1.

Considering the chemical and elemental analysis (Table 2, Fig. 9), DS_1 had higher salt and lower TC content in comparison to DS_2. From July to November, the salt content of the dust samples followed a decreasing trend (EC reduced on average from 35.0 to 2.6 dS/m) while TC increased (Table 2) which agrees with the lesser contribution of DS_1 to the dust composition. In other words, the high salt content of the dust samples during July and August, originates from DS_1 while due to lower activity of DS_1 towards the end of the dry season, DS_2 becomes the dominant dust source, leading to the lower EC and higher TC contents in D_O and D_N dust samples. DS_1 also consisted of higher clay and silt fractions than DS_2, hence the decrease in the clay content of the dust samples from the beginning of the dry season towards the wet season (on average from 2.8% to 0.5%), could also be related to lesser DS_1 activity.

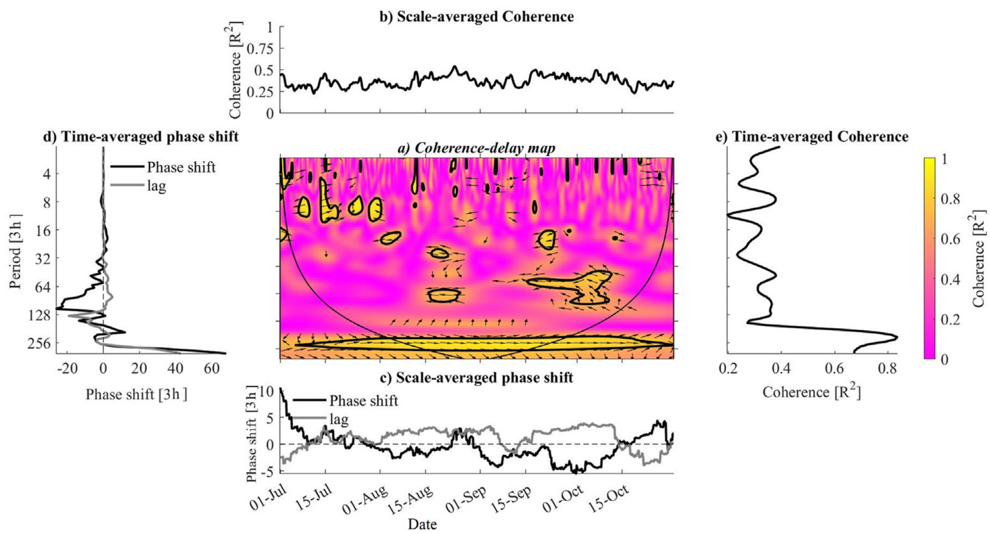

Fig. 12. Coherence-delay plots between PM_{10} at Urmia station and wind speed from the west which is blown over dust sources in Iraq toward the city of Urmia. (a) Coherence-delay map, (b) scale-averaged coherence, (c) scale-averaged phase shift, (d) time-averaged phase shift, and (e) time-averaged coherence.

Table 3
Physical characteristics of SA induced crusts on two soil samples (DS_1 and DS_2) from sand sheets using three methods of application: DSp, WSp, and MC.

SA application	Soil sample	SA conc. (%)	Crust thickness (cm)	Compressive strength (kPa)	
				Mean	Maximum
DSp	DS_1	DSp-SA_0	0.14	487.27	1,589.83
		DSp-$SA_{0.5}$	1.16	2,516.03	6,265.82
		DSp-SA_1	0.83	1,110.30	3,489.50
		DSp-SA_2	0.62	1,426.07	4,233.57
	DS_2	DSp-SA_0	0.0	0.0	0.0
		DSp-$SA_{0.5}$	0.78	303.38	447.84
		DSp-SA_1	0.62	225.40	474.33
		DSp-SA_2	0.33	37.00	209.33
WSp	DS_1	WSp-SA_0	0.14	487.27	1,589.83
		WSp-$SA_{0.5}$	1.44	1,938.38	5,805.85
		WSp-SA_1	1.56	868.42	2,703.30
		WSp-SA_2	1.39	737.79	3,076.42
	DS_2	WSp-SA_0	0.0	0.0	0.0
		WSp-$SA_{0.5}$	1.07	122.13	429.76
		WSp-SA_1	1.13	56.66	170.59
		WSp-SA_2	0.33	56.14	242.06
MC	DS_1	MC-SA_0	0.29	243.67	1,634.0
		MC-$SA_{0.5}$	2.49	6,202.33	10,973.0
		MC-SA_1	2.82	5,178.33	11,021.67
		MC-SA_2	2.83	6,693.67	13,275.80
	DS_2	MC-SA_0	0.17	1.17	18.70
		MC-$SA_{0.5}$	2.65	1,055.0	3,534.07
		MCp-SA_1	2.41	2,367.67	5,116.90
		MC-SA_2	2.56	6,459.33	9,932.23

Note: conc. denotes the concentration of SA, DSp refers to the dry spray, WSp refers to the wet spray, and MC refers to mix and compaction.

3.1.4. Sand sheets contribution to PM_{10} in Urmia city

In section 3.1.3, it is shown that DS_1 and DS_2 contribute significantly to the dust composition near sand sheets. To investigate the significance of the impact of dust from sand sheets on the nearby areas, especially on the city of Urmia (the largest city nearby, 35 km away from the sand sheets), a WCA analysis (Fig. 11) was done between PM_{10} at the Urmia station and the wind speed blowing over the sand sheets towards the city of Urmia in the north and northeast directions (WS_{n-ne}) (Fig. A1 in the Appendix). PM_{10} as a mixture of solid particles and liquid droplets in the air poses a potential threat to human health as it enters the respiratory tract and bloodstream. As shown in Fig. 11, there is an almost perfect anti-correlation between PM_{10} and WS_{n-ne} on the monthly time scale (see yellow parts with arrows pointing to the left and slightly sloping downwards as shown in Fig. 11(a), centered on a period of 250 3-h). This simply means that WS_{n-ne} negatively affects the PM_{10} values in the monthly cycles at the Urmia station, with lag values very close to zero. However, a closer look in Fig. 11(a) shows that there also is a strong local correlation between PM_{10} and WS_{n-ne} in the two-day cycle (see yellow areas with right-facing and slightly upward-sloping arrows, centered at 16 3-h periods). This is also evident from Fig. 11(e), where the time-averaged coherence plots show that the first peak is at 250 3-h periods and then at 16 3-h periods. The localized correlations between PM_{10} and WS_{n-ne} are positive with a lag of ~6–~12 h where WS_{n-ne} controls PM_{10}. This confirms the hypothesis that the dust generated in the sand sheets contributes to the PM_{10} concentration at Urmia station at higher frequencies, but not at lower frequencies. In other words, this may mean that the dust generated in the sand sheets may increase the PM_{10} concentration at the Urmia station on shorter time scales but does not contribute much (or more precisely negatively contributes) to the PM_{10} concentration at the Urmia station on longer time scales. This is plausible because the distance between the sand sheets and the Urmia station is short enough (35 km) for winds from the north and northeast to blow

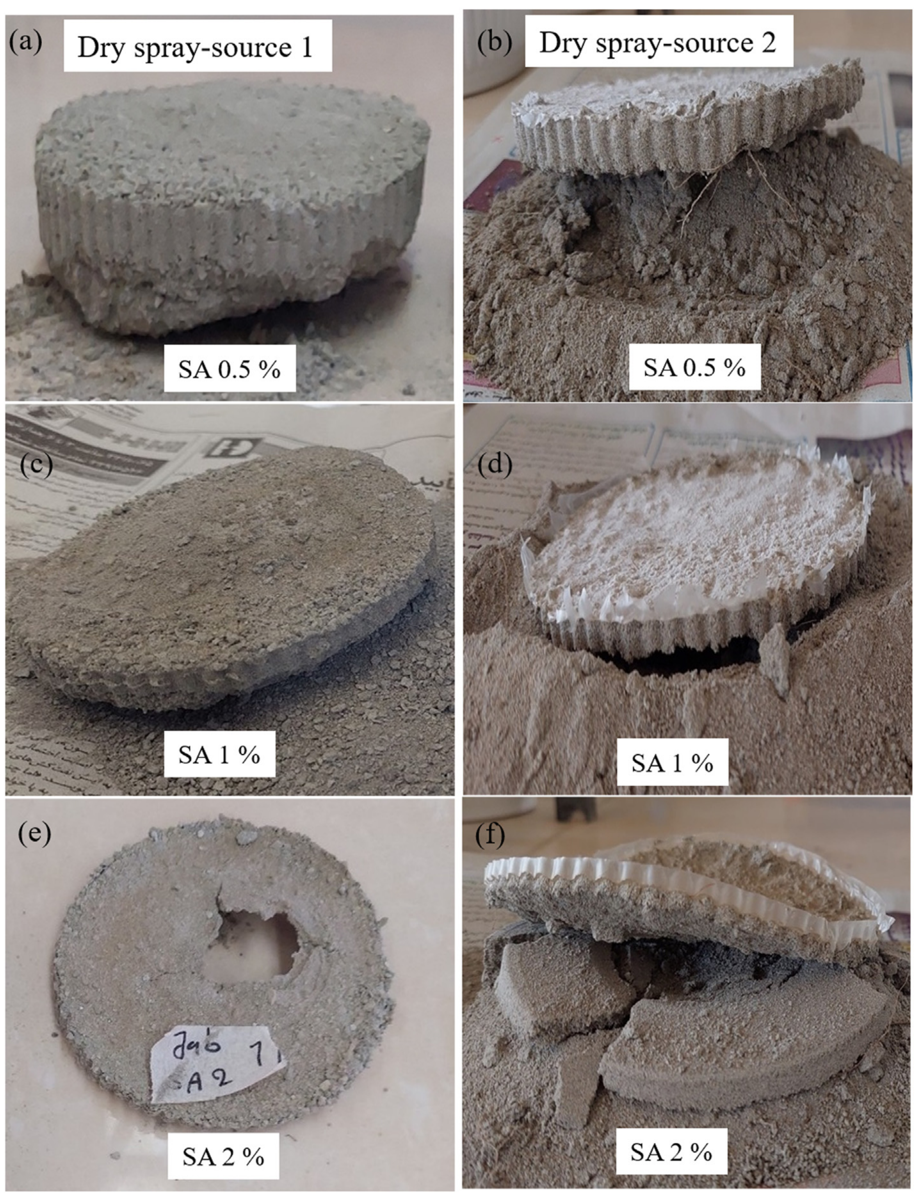

Fig. 13. Crusts developed on soil samples from sand sheets of western Lake Urmia using dry spray method (DSp) and different concentrations of sodium alginate (SA). The left column shows crusts developed on dust source 1 (DS_1), and the right column shows crusts developed on dust source 2 (DS_2).

the accompanying dust out of the city of Urmia at longer time scales.

It appears that another important factor may contribute to the dust concentrations at the Urmia station for longer periods. To check this, another WCA (Fig. 12) was done between PM_{10} and the wind speed blowing from the most common wind direction towards the city of Urmia (West, WS_w, which is most likely blowing over the dust sources in Iraq) (Fig. A1 in the Appendix). Interestingly, the results in Fig. 12 show that there is an almost perfect correlation between PM_{10} and WS_w in the monthly cycle, which means that dust from the westerly direction is probably the main source of dust at the Urmia station on longer time scales. However, in contrast to PM_{10}–WS_{n-ne}, the localized higher correlations at higher frequencies are less dominant in the case of PM_{10}–WS_w.

3.2. Dust source stabilization by sodium alginate

3.2.1. Crust thickness, maximum and mean compressive strength

The results of the different methods of SA application on the physical characteristics of the developed crusts at DS_1 and DS_2 are listed in Table 3. Fig. 13 shows the images of the crusts developed on the surface of the two investigated soils using DSp. In Figs. A2 and A3 in the Appendix, the images of the SA-induced crusts using WSp and the mix and MC methods are respectively shown.

In soil sample DS_1 unlike DS_2, a spray of pure water (Sp-SA_0) led to the development of crusts with an average thickness of 0.14 cm (Table 3; Fig. 14(a)). As described earlier, such crusts were also observed in some parts of DS_1 in the field, and are related to the existence of clay, silt, and NaCl in the sample (Hamzehpour & Marcolli, 2024). However, for MC-SA_0, crusts with a mean thickness of 0.17 cm formed on DS_2, and those of DS_1 were thicker in comparison to Sp-SA_0 (0.29 cm) (Table 3; Figs. 15(a) and 15(b)). The thickest crusts induced by spray methods were observed for DSp-$SA_{0.5}$ with 1.16 and 0.78 cm for DS_1 and DS_2, respectively (Table 3; Figs. 14(a) and 14(b)).

For DS_1, in accordance with the crust thickness results, the highest mean and maximum compressive strength were measured in DSp-$SA_{0.5}$ with the values of 2516.03 and 6265.82 kPa, respectively (Table 3; Figs. 14(c) and 14(e)). For DS_2, the highest mean compressive strength also was measured for DSp-$SA_{0.5}$ with a value of 303.38 kPa, while the maximum compressive strength was found for DSp-SA_1 with a value of 474.33 kPa (Table 3; Figs. 14(d) and 14(f)). By comparing the results of the crusts developed in the DSp method for the two soils, it can be clearly seen that not only the thickness of the crusts developed, but also their compressive strength is significantly different, and the crusts developed on DS_1 are thicker and more stable than those on DS_2 (Fig. 14).

Taking into account spraying of SA on soils at optimum moisture content (WSp), for both soils, the maximum crust thickness was observed for WSp-SA_1 with values of 1.56 and 1.13 cm for DS_1 and DS_2 soils, respectively (Table 3; Figs. 14(a) and 14(b)). Which were 0.40 and 0.35 cm thicker compared to the DSp method. Similar to the DSp results, the highest mean and maximum compressive

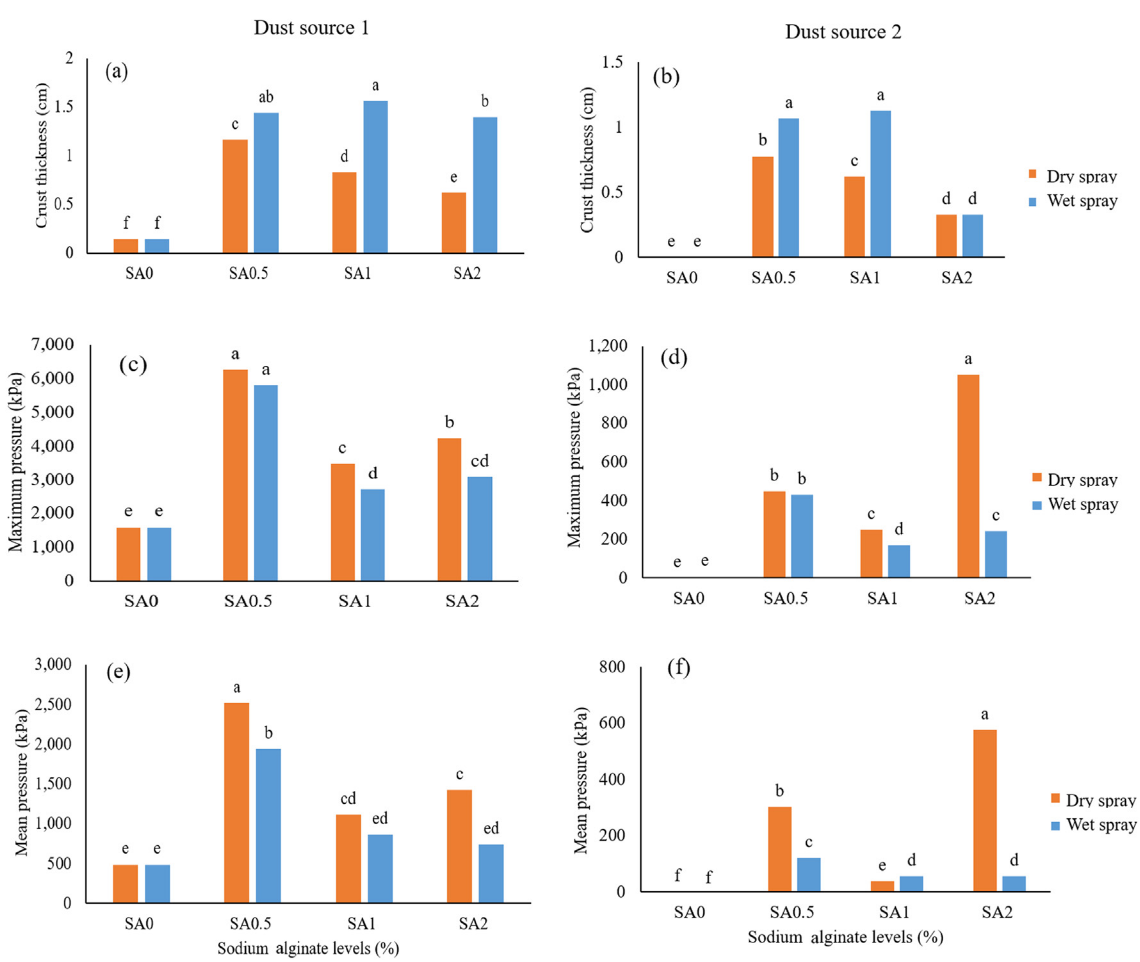

Fig. 14. Mean comparison for the crust thickness, at the mean and maximum compressive strength on two soils from sand sheets of western LU using DSp and WSp methods with four SA concentrations (0%, 0.5%, 1%, and 2%). The left column shows results for DS_1, and the right column shows results for DS_2.

strength in the WSp method was observed for WSp-$SA_{0.5}$ for both soils with mean and maximum compressive strength values of 1938.38 and 5805.85 kPa, respectively, for DS_1, and 122.13 and 429.76 kPa for DS_2 (Table 3; Figs. 14(c) and 14(f)). However, for both soils, the WSp method resulted in thicker crusts (Fig. A2 in the Appendix), while the compressive strength of the crusts was reduced. The reason for the reduction in compressive strength for WSp at all concentrations could be related to the greater penetration depth of the sprayed solution in the WSp treatments due to the presence of initial moisture, which helped the SA solution to penetrate deeper into the soils.

Unlike the Sp methods, crust thickness and the mean and maximum compressive strength for the MC method increased with increasing SA concentration and reached the highest level in SA_2 (Table 3; Fig. 15). The maximum crust thickness for DS_1 was 2.83 cm with the mean and maximum compressive strength of 6693.67 and 13275.80 kPa, respectively (Table 3; Figs. 15(a), 15(c), and 15(e)). For DS_2, these values were 2.56 cm, 6459.33, and 9932.23 kPa, respectively (Table 3; Figs. 15(b), 15(d), and 15(f)). The observed results for the MC method were significantly better than those observed for WSp and DSp methods for both soils, indicating the better performance of the MC method in soil stabilization (Fig. 15). In general, DS_1 responded better to SA application than DS_2 for all methods of applications and concentrations due the higher percentage of clay, silt, primary organic matter, and NaCl which promoted the formation of stable crusts in combination with SA and ultimately lead to the formation of stronger crusts on the surface of DS_1.

The penetration force versus penetration depth graphs for the crusts developed are shown in Fig. 16. For most of the treatments on both soils, the penetration force increased to a depth of 5–10 mm and then decreased reaching the bottom of the crust. However, the crust penetration force had more variation in DS_2 with respect to the depth for the Sp methods (Figs. 16(b) and 16(d)) and reached its minimum value at a depth of 8 mm for DS_2 while for DS_1, the minimum penetration force was at a depth of > 1.5 mm. Nevertheless, similar to the results presented in previous sections, the depth-related penetration force of the MC crusts also was much better than those observed for the Sp methods for all concentrations and followed a monotonous decrease towards the bottom of the crusts, indicating the greater stability of the crusts in deeper layers for MC than for Sp on both DS_1 and DS_2.

A minimum increase of 345 kPa is recommended to consider an additive as an effective stabilizer against wind erosion (ASTM, 2008). Based on this criterion, SA treatment could successfully increase resilience for both soils and all three methods of application with more promising results for DS_1. Even though the MC method showed a significantly better performance than the Sp methods, however, due to the difficulty of soil mixing with SA and then compaction on a large scale in the field, the SA surface spray method is a more practical method and could be considered more economical. Regarding the results of SA spray on the soil surface, DSp-$SA_{0.5}$ and WSp-SA_1 led to thicker and more stable crusts. However, the mean and maximum compressive strength of the crusts were at their highest level for Sp-$SA_{0.5}$ for both soils. Hence, if

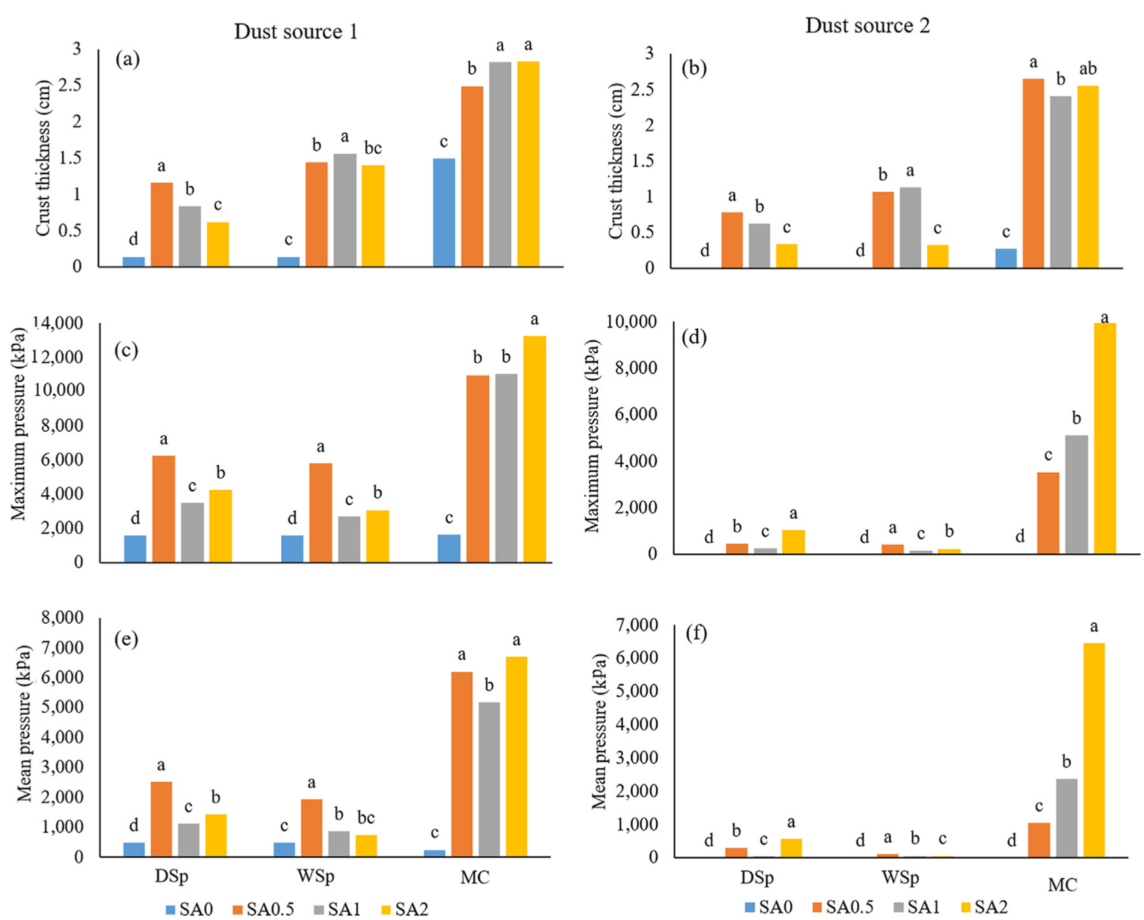

Fig. 15. Mean comparison for crust thickness, and the mean and maximum compressive strength on two soils from the sand sheets of western Lake Urmia using three methods of DSp, WSp, and MC with four SA concentrations (0%, 0.5%, 1%, and 2%). The left column shows results for DS_1, and the right column shows results for DS_2.

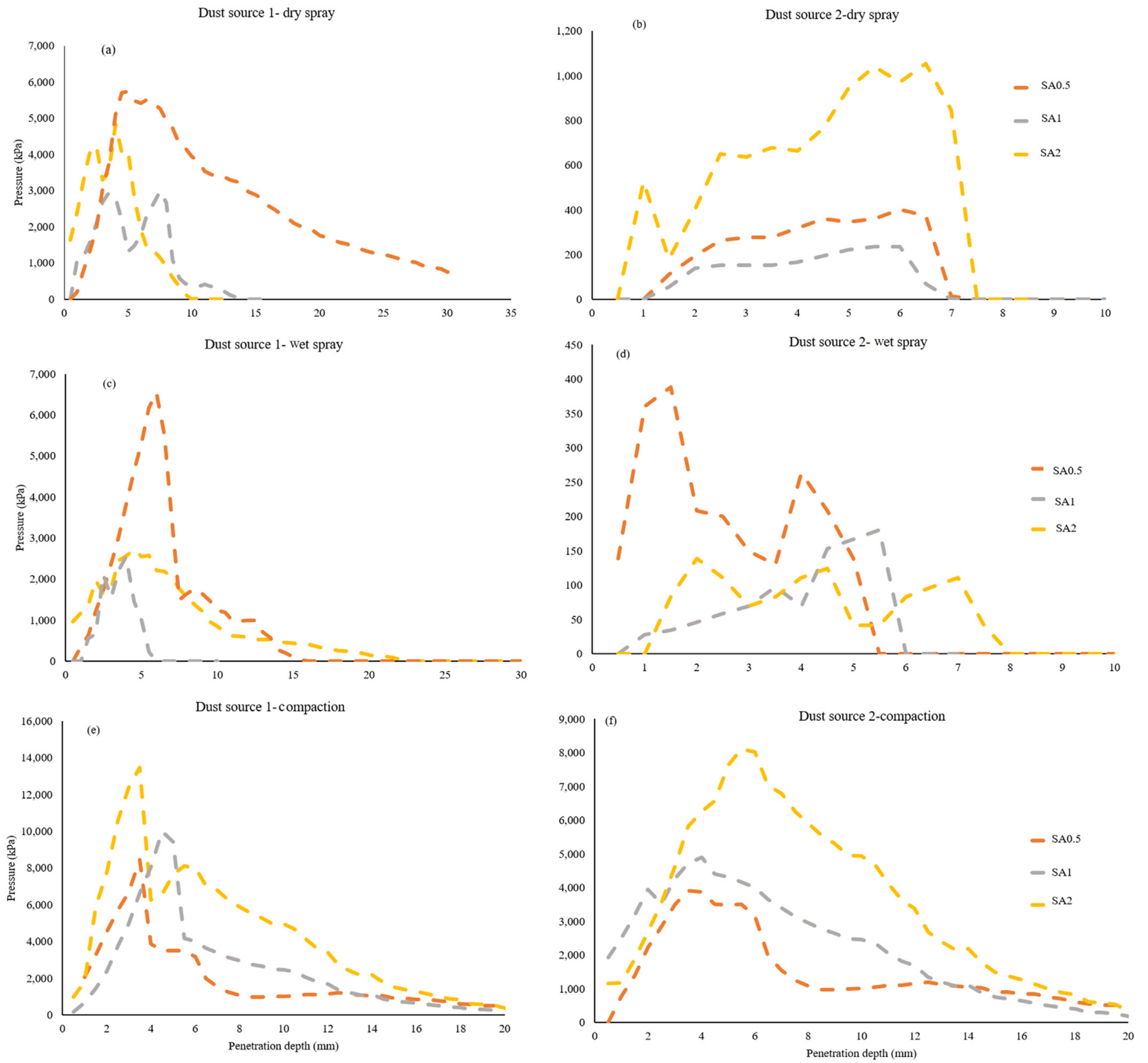

Fig. 16. Penetration force versus penetration depth in crusts developed using sodium alginate solution with four concentration levels (0%, 0.5%, 1%, and 2%) and three methods of sodium alginate applications (wet spray, dry spray, and compression). (a) and (b) dry spray; (c) and (d) wet spray; (e) and (f) mixing with soil and compaction.

the spray method is used, based on the current lab-scale results, it seems that SA spray on the soil after the last stage of spring rains and when the soil has reached the optimal moisture content can lead to more acceptable results for DS_1 while for DS_2, DSp can induce more stable crusts.

Lemboye et al. (2021) reported that the use of agriculturally derived (non-toxic) biopolymers such as SA can improve the resilience of sand dunes against wind speeds up to 16.2 m/s. Arab et al. (2019) used SA to improve the pavement structure in weak cohesive soils. They showed that the use of 2% and 4% SA on the soil surface with silt and clay textures, respectively, significantly improved their resilience modulus. The increased cross-linking between particles, and, thus, soil stiffness due to the presence of SA was confirmed by means of TGA, SEM, and FTIR.

3.2.2. Crust morphology and stability after 3 months

The SEM images of DSp-SA_0 and DSp-SA_1 induced crusts after three months of treatment are shown in Figs. 17 and 18, parts of Figs. 17(a)–17(d) and 18(a)–18(d). By comparing the results of the SA-treated samples (Figs. 17(a)–17(d) and 18(a)–18(d)) with those of untreated samples (Figs. 17(e) and 17(f), 18(e) and 18(f)), it can be seen that SA has formed a continuous layer covering the entire surface of the particles in both soils. By creating a connection and bridges between coarse and fine soil particles, SA has helped to form a crust on the surface of the soil particles. These images show that three months after SA application, SA remained on the soil surface and effectively maintained the bonds between particles, increasing their resilience against wind force.

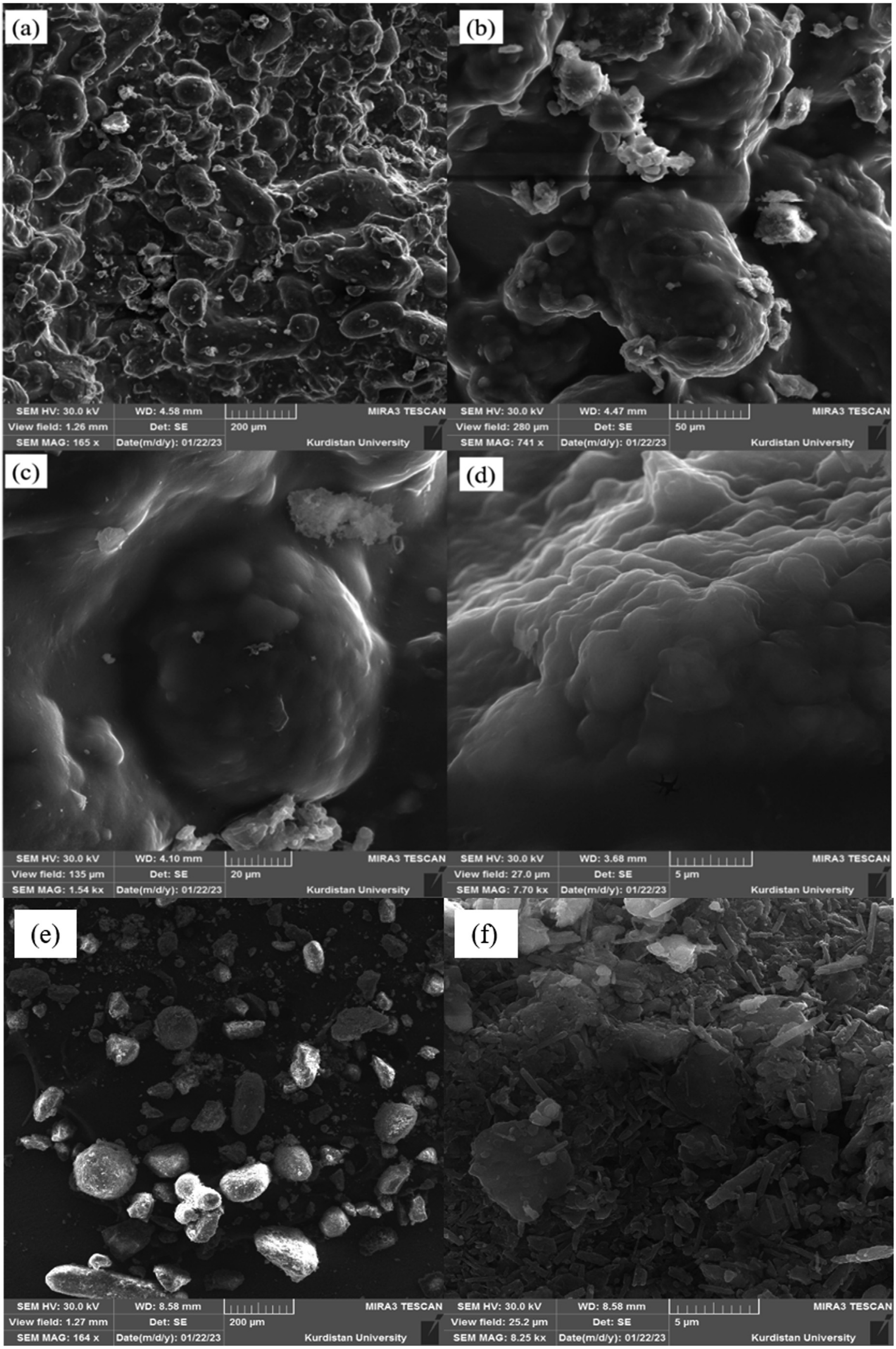

Fig. 17. Scanning electron microscope (SEM) images of crusts developed on surface of DS_1 three months after DSp of SA_1. Images are taken at different magnifications. Sodium alginate masks entire surface of particles including pore spaces. (a) 165X, (b) 741X, (c) 1,540X, and (d) 7,700X. SEM images of untreated DS_1 in (e) 164X and (f) 8,250X magnifications.

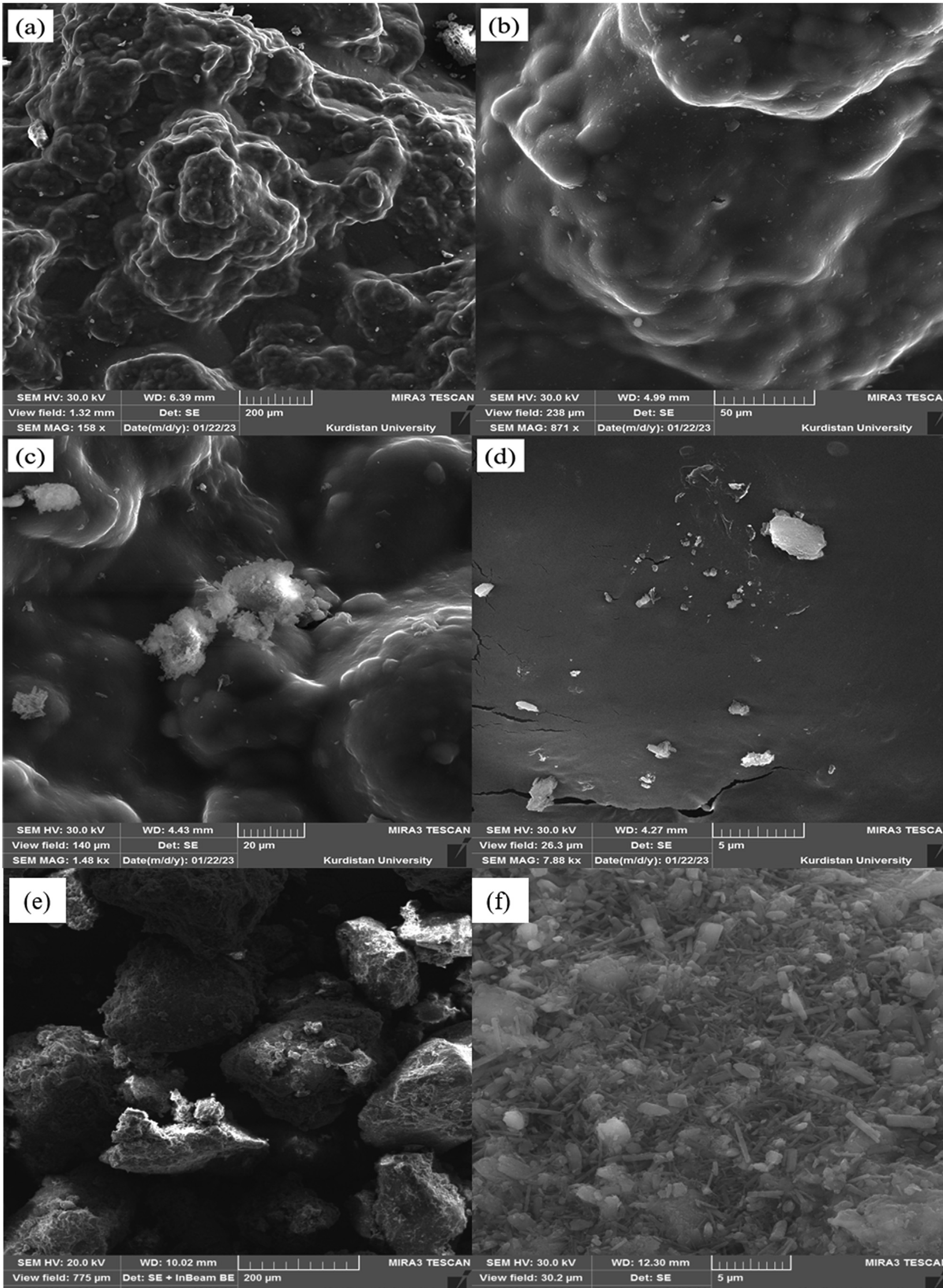

Fig. 18. Scanning electron microscope (SEM) images of crusts developed on surface of DS_2 three months after DSp of SA_1. Images are taken at different magnifications. Sodium alginate masks entire surface of particles including pore spaces. (a) 158X, (b) 871X, (c) 1,480X, and (d) 7,880X. SEM images of untreated DS_2 in (e) 268X and (f) 6,860X magnifications.

Zhao et al. (2020) showed that the use of SA on loess soil, resulted in the formation of larger particles by flocculation via filling the pores between soil particles. SA could also improve the strength, shear parameters, and water stability of loess. Wade et al. (2021) also by using SA on the soil surface improved soil aggregate diameter 1.5 times through which soil susceptibility to wind erosion decreased. Peng et al. (2017) used SA to improve the biological soil crust development on sand to enhance its stabilization. Peng et al. (2017) work showed that SA can form a thin layer on the soil surface, and, therefore, enhance the compressive strength of topsoil without showing negative effects on soil physicochemical properties.

In Fig. 19, the concentration of oxygen (O), carbon (C), sodium (Na), and silicon (Si) calculated from EDX analysis (Fig. A4 in the Appendix) are depicted for DSp_0 and DSp_1 treatments for both DS_1 and DS_2. O, C, and Na are the prevailing elements in the SA composition, and, thus, an increase in their concentration in $DSp\text{-}SA_1$ in comparison to $DSp\text{-}SA_0$ can be an indicator of the SA presence while the concentration of Si is attributed to the mineral portion of the soil samples, and, thus, should not change considerably among $DSp\text{-}SA_0$ and $DSp\text{-}SA_1$ treatments. Taking into consideration Fig. 19, for both soils, in $DSp\text{-}SA_1$, O, C, and to a lesser extent Na, have significantly increased in comparison to $DSp\text{-}SA_0$ whereas the Si concentration remained almost unchanged among the samples. These results are strong confirmation of the SEM images and indicate that three months after a spray of SA solution on both soils, SA could still act effectively as a cement among loose soil particles and increase their resilience to wind erosion by masking and bounding sand size and silt particles. Needle-shaped minerals in untreated samples (Figs. 17(e) and 18(e)) are authigenic aragonite minerals with more dominancy in DS_2 which are completely covered and immobilized by SA, leading to their effectively reduced contribution to dust composition.

In Fig. 20, the TGA thermographs of $DSp\text{-}SA_0$ and $DSp\text{-}SA_1$ treatments for both soils are shown. The weight loss in the range of 150–350 °C can be attributed to the decomposition of easily degradable organic substances such as SA molecules, which are polysaccharide molecules. Weight loss of roughly 3% in $DS_1\text{-}SA_1$ versus 0.7% in $DS_1\text{-}SA_0$ and 1% in $DS_2\text{-}SA_1$ versus 0% for $DS_2\text{-}SA_0$, could then be related to the decomposition of the existing SA molecules.

The weight loss of the samples due to heat up to 150 °C is related to the loss of water molecules absorbed by the soil. In spite of low SA content, according to Fig. 20, it can be seen that the water-holding capacity of both soils has improved quiet well with the presence of SA and under the same conditions, the amount of water retained by SA_1 for DS_1 is much higher than that for DS_2. The amount of water evaporated at a temperature

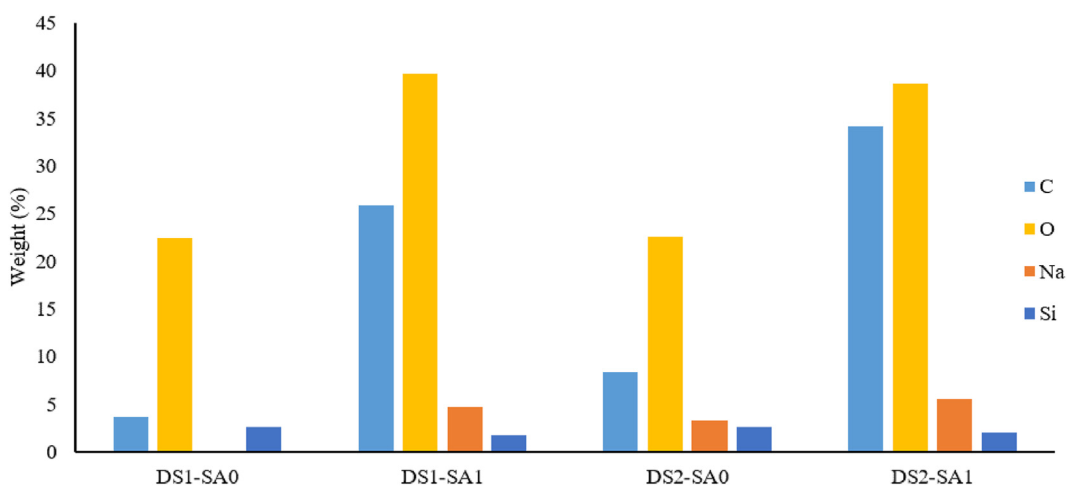

Fig. 19. Concentration of four elements in percent by weight (%) calculated from energy dispersive spectroscopy (EDS) spot analysis. Increase in carbon (C), oxygen (O), and sodium (Na) concentrations in sodium alginate (SA) treated samples indicates presence of SA related organic compounds.

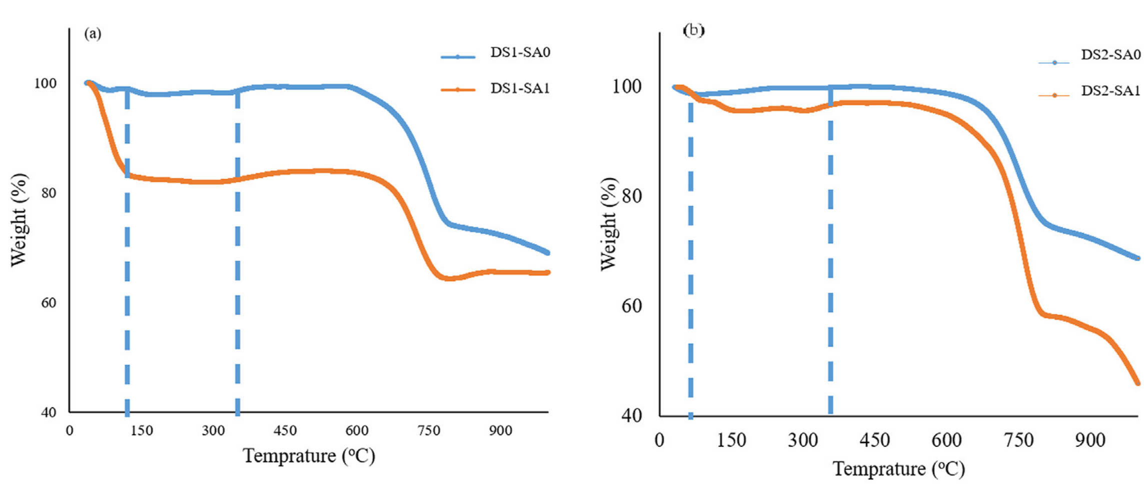

Fig. 20. TGA thermographs for DS_1 and DS_2 three months after applying SA_1 along with untreated samples (SA_0).

below 200 °C in SA_1 and SA_0 treatments for DS_1 was about 17% and 2%, respectively. For DS_2, these values were determined to be roughly 5% and 1%, respectively. The greater water retention for DS_1 could be attributed to the formation of bonds between organic particles and the surfaces of clay and silt particles and the formation of small soil aggregates that help retain more water. The hydrophilic functional groups on SA can also enhance water sorption. Therefore, maintaining 15% more moisture in sample DS_1 and 4% for DS_2 in SA-treated samples in comparison to untreated samples could be related to the presence of SA organic molecules. Arab et al. (2019) have also reported higher water retention capability of sodium alginate biopolymer-treated soil samples.

4. Summary and conclusions

A comprehensive study of the soil and dust samples from the sand sheet playa surface of western Lake Urmia was done during the summer-autumn 2020 to investigate the soil-dust properties, temporal variability in dust characteristics, and dust source stabilization using sodium alginate solution with different concentrations and methods of application. Two previously identified soil types from sand sheets were collected during August 2020, along with the dust collection from July and August (the beginning of the dry season), and October and November (the beginning of the wet season). Two prevailing soil types (DS_1 and DS_2) with high susceptibility to wind erosion from sand sheets were significantly different in terms of electrical conductivity (EC), organic matter content (OM), total carbonates (TC), and particle size distribution. Calcium (Ca), magnesium (Mg), sodium (Na), silicon (Si), iron (Fe), and aluminum (Al) were found to be the most dominant elements in both soil and dust samples. XRF results also confirmed that CaO, SiO_2, and Na_2O are the common elemental compounds in the samples.

The coefficient of determination (R^2) between existing elements in the soil and dust samples revealed that both selected soil samples are major sources of the airborne dust, indicating the local contribution of the soils to the dust in the region. However, the higher R^2 for DS_1 during July and August and on the contrary, greater values for DS_2 during October and November confirm that at the beginning of the dry season in the region, DS_1 contributes more to dust composition while towards the beginning of the wet season, DS_1 becomes less active and DS_2 becomes the major contributor to dust composition. Correlation wavelet analysis between PM_{10} at the Urmia station and the wind speed blowing over the sand sheets towards the city of Urmia (WS_{n-ne}) showed that there is a strong local correlation between PM_{10} and wind speeds with north-northeast direction in a two-day cycle. In other words, the localized correlations between PM_{10} and WS_{n-ne} are positive with a lag from ~6 to ~12 h where WS_{n-ne} controls PM_{10}. This confirms the hypothesis that the dust generated from the sand sheets contributes to the PM_{10} concentration at the Urmia station at higher frequencies, but not at lower frequencies.

The absence of NaCl in the sediment of DS_2, along with the significant differences in the soil basic properties between DS_1 and DS_2 with higher values of salinity, OM, clay, and silt fractions for DS_1, provides a favorable condition for the development of a surface crust which prevents the surface of soil DS_1 from further erosion. Each year after the wet season, sodium chloride accumulates on the surface of DS_1 due to its capillary movement from the lower layers to the surface parallel to the soil's water evaporation towards middle-dry season. Thus, towards the end of the dry season in the region, DS_2 with no surface crust nor vegetation cover becomes the sole dust origin up to the end of November. The application of sodium alginate (SA) on both soils, lead to acceptable results by means of crust development and wind resistance with better results for DS_1 than DS_2. It seems that the higher silt, clay, and salt content of DS_1 improves the performance of the SA solution by increasing the stability and thickness of the crusts developed. Among the three methods of SA application, soil mix with SA solution and compaction (MC) yielded significantly better results than wet (WSp) and dry (DSp) spray for both soils. However, taking into consideration the time required and the high costs of the MC method, either DSp (when the soil is completely dry in the field) or WSp (after the very last rainfall) with 0.5%–1% concentration are more advisable for application in the field to improve soil stability against wind as well as water retention capacity. SA-induced crusts remain stable at least up to three months after application as proved by SEM-EDX and TGA analysis. As the extremely dry season in the region is roughly 4 months (July to October), SA-induced crusts can reasonably act as a cement thoroughly holding the sand size particles, increasing their resistance against wind forces.

Author contributions

NH did the research design, lab experiments, and field work. NH prepared the manuscript. GRM sis to the research design and interpretation of lab analysis. MR conducted the correlation wavelet analysis along with the discussion of the results and writing the related sections.

Declaration of competing interest

The authors declare that they have no known competing financial interests or personal relationships that could have appeared to influence the work reported in this paper.

Acknowledgements

This research is based upon research funded by Iran National Science Foundation (INSF), under project No. 4005422.

Appendix A. Supplementary data

Supplementary data to this article can be found online at https://doi.org/10.1016/j.ijsrc.2024.04.003.

References

Afrin, H. (2017). A review on different types soil stabilization techniques. *International Journal of Transportation Engineering and Technology, 3*(2), 19–24.
Ahmady-Birgani, H., Mirnejad, H., Feiznia, S., & McQueen, K. G. (2015). Mineralogy and geochemistry of atmospheric particulates in western Iran. *Atmospheric Environment, 119*, 262–272.
Ahmady-Birgani, H., Agahi, E., Ahmadi, S. J., & Erfanian, M. (2018). Sediment source fingerprinting of the Lake Urmia sand dunes. *Scientific Reports, 8*(1), 1–15.
Ahmady-Birgani, H., Ravan, P., Schlosser, J. S., Cuevas-Robles, A., AzadiAghdam, M., & Sorooshian, A. (2020). On the chemical nature of wet deposition over a major desiccated lake: Case study for Lake Urmia basin. *Atmospheric Research, 234*, 104762.
Aladin, N. V., Plotnikov, I. S., Micklin, P., & Ballatore, T. (2009). Aral Sea: Water level, salinity and long-term changes in biological communities of an endangered ecosystem-past, present and future. *Natural Resources and Environmental Issues, 15*(1), 177–183.
Al-Dabbas, M. A., Ayad Abbas, M., & Al-Khafaji, R. M. (2012). Dust storms loads analyses—Iraq. *Arabian Journal of Geosciences, 5*(1), 121–131.
Alkhayer, M., Eghbal, M. K., & Hamzehpour, N. (2019). Geomorphic surfaces of eastern lake Urmia Playa and their influence on dust storms. *Journal of Applied Sciences & Environmental Management, 23*(8), 1511–1520.
Almajed, A., Lemboye, K., Arab, M. G., & Alnuaim, A. (2020). Mitigating wind erosion of sand using biopolymer-assisted EICP technique. *Soils and Foundations, 60*(2), 356–371.

American Society for Testing and Materials (ASTM). (2008). *Standard guide for evaluating effectiveness of admixtures for soil stabilization*. U.S: ASTM International.

Arab, M. G., Mousa, R. A., Gabr, A. R., Azam, A. M., El-Badawy, S. M., & Hassan, A. F. (2019). Resilient behavior of sodium alginate–treated cohesive soils for pavement applications. *Journal of Materials in Civil Engineering, 31*(1), 04018361.

Bacon, S. N., Burke, R. M., Pezzopane, S. K., & Jayko, A. S. (2006). Last glacial maximum and Holocene lake levels of Owens Lake, eastern California, USA. *Quaternary Science Reviews, 25*(11–12), 1264–1282.

Beaucamp, A., Wang, Y., Culebras, M., & Collins, M. N. (2019). Carbon fibres from renewable resources: The role of the lignin molecular structure in its blendability with biobased poly (ethylene terephthalate). *Green Chemistry, 21*(18), 5063–5072.

Belnap, J., & Büdel, B. (2016). Biological soil crusts as soil stabilizers. In B. weber, B. Büdel, & J. Belnap (Eds.), *Biological soil crusts: An organizing principle in drylands* (pp. 305–320). Berlin: Springer.

Bermanec, V., Posilović, H., & Žigovečki Gobac, Ž. (2009). Identification of biogenetic calcite and aragonite using SEM. *Geologia Croatica, 62*(3), 201–206.

Bishop, J. K., Davis, R. E., & Sherman, J. T. (2002). Robotic observations of dust storm enhancement of carbon biomass in the North Pacific. *Science, 298*(5594), 817–821.

Boroughani, M., Hashemi, H., Hosseini, S. H., Pourhashemi, S., & Berndtsson, R. (2019). Desiccating Lake Urmia: A new dust source of regional importance. *IEEE Geoscience and Remote Sensing Letters, 17*(9), 1483–1487.

Chan, L. W., Lee, H. Y., & Heng, P. W. (2006). Mechanisms of external and internal gelation and their impact on the functions of alginate as a coat and delivery system. *Carbohydrate Polymers, 63*(2), 176–187.

Clarke, A. D., Collins, W. G., Rasch, P. J., Kapustin, V. N., Moore, K., Howell, S., & Fuelberg, H. E. (2001). Dust and pollution transport on global scales: Aerosol measurements and model predictions. *Journal of Geophysical Research: Atmospheres, 106*(D23), 32555–32569.

Colazo, J. C., & Buschiazzo, D. E. (2010). Soil dry aggregate stability and wind erodible fraction in a semiarid environment of Argentina. *Geoderma, 159*(1–2), 228–236.

Dane, J. H., & Topp, C. G. (Eds.). (2020). *Methods of soil analysis, Part 4: Physical methods, 20*. New York: John Wiley & Sons.

Díaz-Hernández, J. L., Martín-Ramos, J. D., & López-Galindo, A. (2011). Quantitative analysis of mineral phases in atmospheric dust deposited in the south–eastern Iberian Peninsula. *Atmospheric Environment, 45*(18), 3015–3024.

Eimanifar, A., & Mohebbi, F. (2007). Urmia Lake (northwest Iran): A brief review. *Saline Systems, 3*(1), 1–8.

Firoozi, A. A., Guney Olgun, C., Firoozi, A. A., & Baghini, M. S. (2017). Fundamentals of soil stabilization. *International Journal of Geo-Engineering, 8*, 1–16.

Fraccaro, L. (2009). An unquenchable thirst: The relationship between water and Owens Valley. *Geology, 190*, 17.

Froyd, K. D., Yu, P., Schill, G. P., Brock, C. A., Kupc, A., Williamson, C. J., … Murphy, D. M. (2022). Dominant role of mineral dust in cirrus cloud formation revealed by global-scale measurements. *Nature Geoscience, 15*(3), 177–183.

Galloza, M. S., Webb, N. P., Bleiweiss, M. P., Winters, C., Herrick, J. E., & Ayers, E. (2018). Exploring dust emission responses to land cover change using an ecological land classification. *Aeolian Research, 32*, 141–153.

Grinsted, A., Moore, J. C., & Jevrejeva, S. (2004). Application of the cross wavelet transform and wavelet coherence to geophysical time series. *Nonlinear Processes in Geophysics, 11*(5/6), 561–566.

Guilherme, M. R., Aouada, F. A., Fajardo, A. R., Martins, A. F., Paulino, A. T., Davi, M. F., … Muniz, E. C. (2015). Superabsorbent hydrogels based on polysaccharides for application in agriculture as soil conditioner and nutrient carrier: A review. *European Polymer Journal, 72*, 365–385.

Hamzehpour, N., & Marcolli, C. (2024). Soil crust development on different playa surfaces of Lake Urmia and its controlling factors-an insight to combat dust sources. *Catena, 237*, 107744.

Hamzehpour, N., Marcolli, C., Klumpp, K., Thöny, D., & Peter, T. (2022). The Urmia Playa as source of airborne dust and ice nucleating particles–Part 2: Unraveling the relationship between soil dust composition and ice-nucleation activity. *Atmospheric Chemistry and Physics, 22*, 14931–14956.

Hamzehpour, N., Marcolli, C., Pashai, S., Klumpp, K., & Peter, T. (2022). The Urmia Playa as source of airborne dust and ice nucleating particles–Part 1: Correlation between soils and airborne samples. *Atmospheric Chemistry and Physics, 22*, 14905–14930.

Hassan, A., Ilyas, S. Z., Agathopoulos, S., Hussain, S. M., Jalil, A., Ahmed, S., & Baqir, Y. (2021). Evaluation of adverse effects of particulate matter on human life. *Heliyon, 7*(2), e05968.

Ingles, O. G., & Metcalf, J. B. (1972). *Soil stabilization principles and practice*. New York: Wiley.

Jiries, A., El-Hasan, T., & Manasrah, W. (2002). Qualitative evaluation of the mineralogical and chemical composition of dry deposition in the central and southern highlands of Jordan. *Chemosphere, 48*(9), 933–938.

Ju, T., Li, X., Zhang, H., Cai, X., & Song, Y. (2018). Effects of soil moisture on dust emission from 2011 to 2015 observed over the Horqin Sandy Land area, China. *Aeolian Research, 32*, 14–23.

Kelts, K., & Hsü, K. J. (1978). Freshwater carbonate sedimentation. In *Lakes: Chemistry, geology, physics* (pp. 295–323). New York: Springer.

Kelts, K., & Shahrabi, M. (1986). Holocene sedimentology of hypersaline Lake Urmia, northwestern Iran. *Palaeogeography, Palaeoclimatology, Palaeoecology, 54*(1–4), 105–130.

Kheirfam, H. (2022). Spatial prioritization of wind-erosion-prone areas in the dried-up beds of Lake Urmia: Using field sampling and in-vitro measurement. *Catena, 217*, 106507.

Kilic, O., & Kilic, A. M. (2010). Salt crust mineralogy and geochemical evolution of the Salt Lake (Tuz Gölü), Turkey. *Scientific Research and Essays, 5*(11), 1317–1324.

Kim, H., & Choi, M. (2015). Impact of soil moisture on dust outbreaks in East Asia: Using satellite and assimilation data. *Geophysical Research Letters, 42*(8), 2789–2796.

Labat, D. (2005). Recent advances in wavelet analyses: Part 1. A review of concepts. *Journal of Hydrology, 314*(1–4), 275–288.

Lahalih, S. M., & Ahmed, N. (1998). Effect of new soil stabilizers on the compressive strength of dune sand. *Construction and Building Materials, 12*(6–7), 321–328.

Lak, R., Mohammadi, A., & Darvishi Khatooni, J. (2021). Lake Urmia brine evolution from 2007 to 2019. In *The handbook of environmental chemistry*. Berlin: Springer.

Lemboye, K., Almajed, A., Alnuaim, A., Arab, M., & Alshibli, K. (2021). Improving sand wind erosion resistance using renewable agriculturally derived biopolymers. *Aeolian Research, 49*, 100663.

Li, J., Okin, G. S., Alvarez, L., & Epstein, H. (2007). Quantitative effects of vegetation cover on wind erosion and soil nutrient loss in a desert grassland of southern New Mexico, USA. *Biogeochemistry, 85*(3), 317–332.

Liu, J., Shi, B., Lu, Y., Jiang, H., Huang, H., Wang, G., & Kamai, T. (2012). Effectiveness of a new organic polymer sand-fixing agent on sand fixation. *Environmental Earth Sciences, 65*, 589–595.

Middleton, N. J. (2017). Desert dust hazards: A global review. *Aeolian Research, 24*, 53–63.

Molina, C., Toro, A. R., Manzano, C. A., Canepari, S., Massimi, L., & Leiva-Guzmán, M. A. (2020). Airborne aerosols and human health: Leapfrogging from mass concentration to oxidative potential. *Atmosphere, 11*(9), 917.

Motaghi, F. A., Hamzehpour, N., Abasiyan, S. M. A., & Rahmati, M. (2020). The wind erodibility in the newly emerged surfaces of Urmia Playa Lake and adjacent agricultural lands and its determining factors. *Catena, 194*, 104675.

Munkhtsetseg, E., Shinoda, M., Gillies, J. A., Kimura, R., King, J., & Nikolich, G. (2016). Relationships between soil moisture and dust emissions in a bare sandy soil of Mongolia. *Particuology, 28*, 131–137.

Nelson, D. W., & Sommers, L. E. (1996). Total carbon, organic carbon, and organic matter. In *Methods of soil analysis: Part 3 chemical methods* (pp. 961–1010). Madison: Soil Science Society of America.

Nield, J. M., Bryant, R. G., Wiggs, G. F., King, J., Thomas, D. S., Eckardt, F. D., & Washington, R. (2015). The dynamism of salt crust patterns on playas. *Geology, 43*(1), 31–34.

Page, A. L., Miller, R. H., & Keeney, D. R. (1982). *Methods of soil analysis: Chemical and microbiological properties* (Vol. 2). Medison: American Society of Agronomy.

Peng, C., Zheng, J., Huang, S., Li, S., Li, D., Cheng, M., & Liu, Y. (2017). Application of sodium alginate in induced biological soil crusts: Enhancing the sand stabilization in the early stage. *Journal of Applied Phycology, 29*(3), 1421–1428.

Pierre, C., Bergametti, G., Marticorena, B., Mougin, E., Bouet, C., & Schmechtig, C. (2012). Impact of vegetation and soil moisture seasonal dynamics on dust emissions over the Sahel. *Journal of Geophysical Research: Atmospheres, 117*(D6), D06114.

Prandel, L. V., Saab, S. C., Brinatti, A. M., Giarola, N. F. B., Leite, W. C., & Cassaro, F. A. M. (2014). Mineralogical analysis of clays in hardsetting soil horizons, by X-ray fluorescence and X-ray diffraction using Rietveld method. *Radiation Physics and Chemistry, 95*, 65–68.

Rahi, A., Rahmati, M., Dari, J., Saltalippi, C., Brogi, C., & Morbidelli, R. (2023). Unraveling hydroclimatic forces controlling the runoff coefficient trends in central Italy's Upper Tiber Basin. *Journal of Hydrology: Regional Studies, 50*, 101579.

Rahmati, M., Groh, J., Graf, A., Pütz, T., Vanderborght, J., & Vereecken, H. (2020). On the impact of increasing drought on the relationship between soil water content and evapotranspiration of a grassland. *Vadose Zone Journal, 19*(1), e20029.

Rai, P. K. (2015). Multifaceted health impacts of particulate matter (PM) and its management: An overview. *Environmental Skeptics and Critics, 4*(1), 1–26.

Rai, P. K. (2016). Impacts of particulate matter pollution on plants: Implications for environmental biomonitoring. *Ecotoxicology and Environmental Safety, 129*, 120–136.

Rashki, A., Eriksson, P. G., Rautenbach, C. D. W., Kaskaoutis, D. G., Grote, W., & Dykstra, J. (2013). Assessment of chemical and mineralogical characteristics of airborne dust in the Sistan region, Iran. *Chemosphere, 90*(2), 227–236.

Rashki, A., Kaskaoutis, D. G., Goudie, A. S., & Kahn, R. A. (2013). Dryness of ephemeral lakes and consequences for dust activity: The case of the Hamoun drainage basin, southeastern Iran. *Science of the Total Environment, 463*, 552–564.

Rezaian Langerodi, S., Lak, R., & Mahdloo Torkamani, S. (2016). Investigation of hydro-geochemistry and brine evolution and sources of Hoz-e-soltan Lake, Qom. *Quaternary Journal of Iran, 2*(1), 79–91.

Rhoades, J. D. (1996). Salinity: Electrical conductivity and total dissolved solids. *Methods of soil analysis: Part 3 Chemical methods, 5*, 417–435.

Ries, J. B., Marzen, M., Iserloh, T., & Fister, W. (2014). Soil erosion in Mediterranean landscapes–experimental investigation on crusted surfaces by means of the portable wind and rainfall simulator. *Journal of Arid Environments, 100*, 42–51.

Saldanha, R. B., Scheuermann Filho, H. C., Mallmann, J. E. C., Consoli, N. C., & Reddy, K. R. (2018). Physical–mineralogical–chemical characterization of carbide lime: An environment-friendly chemical additive for soil stabilization. *Journal of Materials in Civil Engineering, 30*(6), 06018004.

SAS Institute Inc. (2006). *SAS 9.1.3 output delivery system: user's guide, 1–2*.
Schepanski, K. (2018). Transport of mineral dust and its impact on climate. *Geosciences, 8*(5), 151.
Shadkam, S., Ludwig, F., van Vliet, M. T., Pastor, A., & Kabat, P. (2016). Preserving the world second largest hypersaline lake under future irrigation and climate change. *Science of the Total Environment, 559*, 317–325.
Sharifi, A., Shah-Hosseini, M., Pourmand, A., Esfahaninejad, M., & Haeri-Ardakani, O. (2018). The vanishing of Urmia lake: A geolimnological perspective on the hydrological imbalance of the world's second largest hypersaline lake. In P. Ghaffari, & E. V. Yakushev (Eds.), *Lake Urmia* (pp. 41–78). Cham, Germany: Springer.
Siddiqi, R. A., & Moore, J. C. (1981). Polymer stabilization of sandy soils for erosion control. *Transportation Research Record*, (827), 30–34.
Sotoudeheian, S., Salim, R., & Arhami, M. (2016). Impact of middle eastern dust sources on PM10 in Iran: Highlighting the impact of tigris–euphrates basin sources and Lake Urmia desiccation. *Journal of Geophysical Research: Atmospheres, 121*(23), 14018–14034.
Taghizadeh-Mehrjardi, R., Hamzehpour, N., Hassanzadeh, M., Heung, B., Goydaragh, M. G., Schmidt, K., & Scholten, T. (2021). Enhancing the accuracy of machine learning models using the super learner technique in digital soil mapping. *Geoderma, 399*, 115108.
Takigami, H., Taniguchi, N., Shimizu, Y., & Matsui, S. (1998). Toxicity assays and their evaluation on organic polymer flocculants used for municipal sludge dewatering. *Water Science and Technology, 38*(7), 207–215.
Tallarida, R. J., Murray, R. B., Tallarida, R. J., & Murray, R. B. (1987). Duncan multiple range test. *Manual of pharmacologic calculations: With computer programs* (pp. 125–127).
Tegen, I., Harrison, S. P., Kohfeld, K., Prentice, I. C., Coe, M., & Heimann, M. (2002). Impact of vegetation and preferential source areas on global dust aerosol: Results from a model study. *Journal of Geophysical Research: Atmospheres, 107*(D21). AAC-14-1-AAC 14–27.
Wade, E., Zowada, R., & Foudazi, R. (2021). Alginate and guar gum spray application for improving soil aggregation and soil crust integrity. *Carbohydrate Polymer Technologies and Applications, 2*, 100114.
Warrence, N. J., Bauder, J. W., & Pearson, K. E. (2002). Basics of salinity and sodicity effects on soil physical properties. *Department of land resources and environmental sciences*. Bozeman, MT. U.S: Montana State University.
Wilske, B., Bai, M., Lindenstruth, B., Bach, M., Rezaie, Z., Frede, H. G., & Breuer, L. (2014). Biodegradability of a polyacrylate superabsorbent in agricultural soil. *Environmental Science and Pollution Research, 21*(16), 9453–9460.
Wurtsbaugh, W. A., & Sima, S. (2022). Contrasting management and fates of two sister lakes: Great Salt Lake (USA) and Lake Urmia (Iran). *Water, 14*(19), 3005.
Yan, Y., Wu, L., Xin, X., Wang, X., & Yang, G. (2015). How rain-formed soil crust affects wind erosion in a semi-arid steppe in northern China. *Geoderma, 249*, 79–86.
Yang, J., Wang, F., Fang, L., & Tan, T. (2007). Synthesis, characterization and application of a novel chemical sand-fixing agent-poly (aspartic acid) and its composites. *Environmental Pollution, 149*(1), 125–130.
Zarasvandi, A., Carranza, E. J. M., Moore, F., & Rastmanesh, F. (2011). Spatio-temporal occurrences and mineralogical–geochemical characteristics of airborne dusts in Khuzestan Province (southwestern Iran). *Journal of Geochemical Exploration, 111*(3), 138–151.
Zhao, Y., Zhuang, J., Wang, Y., Jia, Y., Niu, P., & Jia, K. (2020). Improvement of loess characteristics using sodium alginate. *Bulletin of Engineering Geology and the Environment, 79*(4), 1879–1891.
Zobeck, T. M., Baddock, M., van Pelt, R. S., Tatarko, J., & Acosta-Martinez, V. (2013). Soil property effects on wind erosion of organic soils. *Aeolian Research, 10*, 43–51.